Journal of Hydrology 614 (2022) 128514

Contents lists available at ScienceDirect

Journal of Hydrology

journal homepage: www.elsevier.com/locate/jhydrol

Research papers

Vegetation greening intensified transpiration but constrained soil evaporation on the Loess Plateau

Fuxiao Jiang [a,b], Xianhong Xie [a,b,*], Yibing Wang [a,b], Shunlin Liang [c], Bowen Zhu [d], Shanshan Meng [e], Xiaotong Zhang [a,b], Yuchao Chen [a,b], Yao Liu [a,b]

[a] State Key Laboratory of Remote Sensing Science, Beijing Normal University, Beijing 100875, China
[b] Beijing Engineering Research Center for Global Land Remote Sensing Products, Institute of Remote Sensing Science and Engineering, Faculty of Geographical Science, Beijing Normal University, Beijing 100875, China
[c] Department of Geography, University of Hong Kong, Hong Kong 999077, China
[d] College of Water Science and Engineering, Taiyuan University of Technology, Taiyuan 030024, China
[e] College of Geography and Environment, Shandong Normal University, Jinan 250014, China

ARTICLE INFO

This manuscript was handled by Marco Borga, Editor-in-Chief, with the assistance of Hanbo Yang, Associate Editor

Keywords:
Soil evaporation
Vegetation transpiration
Vegetation greening
Land surface hydrological modelling
Loess Plateau

ABSTRACT

Global vegetation greenness has likely enhanced evapotranspiration (ET) that has been assumed to be the primary contributor to water consumption in some regions. However, the proportion of each ET component and their changes given vegetation greening are unclear. In this study, we investigated the response of ET components, especially vegetation transpiration (E_t) and soil evaporation (E_s), to vegetation and climate changes in a typical dryland region, i.e., the Loess Plateau in China, where vegetation is significantly greening. We used a sophisticated hydrological model (i.e., the Variable Infiltration Capacity, VIC) to partition ET, which considers the water-energy balance and vegetation dynamics associated with satellite products of fractional vegetation cover, leaf area index, surface albedo, and radiation forcing. The results showed that during the greening period of 2000–2018, E_t had the largest increasing rate among the components and accounted for 31.8% of the ET. In contrast, E_s showed a minor increase but occupied a larger proportion of about 60% of ET. Therefore, water consumption was primarily from E_s rather than E_t despite the increased proportion of E_t. Vegetation greening certainly intensified E_t, but also substantially constrained E_s with a rate of -2.36 mm yr^{-1}. Increasing water availability (i.e., more precipitation) on the Loess Plateau made the largest contribution to the increase in the annual ET compared with vegetation greening and radiation forcing. These findings imply that the effect of vegetation greening on water consumption may be overestimated on the Loess Plateau. Our study highlights the importance of considering water balance and vegetation dynamics when evaluating ecological programs.

1. Introduction

Evapotranspiration (ET) is a major water flux in the energy-carbon–water cycle of ecosystems, transferring 60–90% of precipitation to the atmosphere (Law et al., 2002; Oki and Kanae, 2006). It comprises soil evaporation (E_s) and vegetation-associated evaporation, i.e., vegetation transpiration (E_t) and canopy interception loss (E_c) (Penman and Keen, 1948; Zhang et al., 2019b). Where snow constitutes a significant portion of the total precipitation, sublimation (E_{sn}) is included in this term (Wilcox et al., 2003). E_t and E_s have totally different functions within ecosystems: the former is strongly related to gross ecosystem productivity, whereas the latter does not directly contribute to production (Hu et al., 2008; Schlesinger and Jasechko, 2014). These components have divergent responses to meteorological conditions, soil moisture storage and vegetation coverage (Zhang et al., 2016b).

The factors driving the ET process can be divided into water supply (e.g., precipitation), energy availability (e.g., solar radiation) and vegetation coverage (Monteith, 1965). Precipitation increased in the Northern Hemisphere mid- to high-latitude lands and decreased in some of the tropical and subtropical areas (Adler et al., 2017; Gu, 2016), which resulted in ET changes (Pan et al., 2015). Downward shortwave radiation recovered in many parts of the world after 1980 (Wild, 2016), and downward longwave radiation rose almost everywhere while clustering at the high-latitude in the Northern Hemisphere (Wang and Liang,

* Corresponding author at: State Key Laboratory of Remote Sensing Science, Beijing Normal University, Beijing 100875, China.
E-mail address: xianhong@bnu.edu.cn (X. Xie).

https://doi.org/10.1016/j.jhydrol.2022.128514
Received 14 August 2022; Received in revised form 9 September 2022; Accepted 12 September 2022
Available online 10 October 2022

2009); both of these changes could influence the ET trend (Jiang et al., 2021). In addition to water and energy constraints, vegetation coverage also plays an important role in the terrestrial water cycle that affects ET directly through transpiration and indirectly through determining surface absorbed radiation by albedo changes (Duveiller et al., 2018). Vegetation greening has been increasing globally since 1981 (Piao et al., 2020), which has been assumed to cause global intensification of terrestrial ET (Zeng et al., 2018).

In the context of climate change and vegetation greenness, many studies have been devoted to quantifying the contributions of various factors (e.g., precipitation and vegetation) to ET changes. A few studies reported that climate change, especially precipitation, determined the spatiotemporal variations in ET and elevated atmospheric CO_2 ranked second after 1982 (Mao et al., 2015; Shi et al., 2013). Some studies found that vegetation greening was the primary driver of the global ET increasing trend since 1982 (Zeng et al., 2016; Zhang et al., 2015b). Jung et al. (2010) indicated that increasing soil moisture limitations on ET largely explained the declining trend of the global terrestrial ET during 1998–2008. Zhang et al. (2016b) analysed the effect of greening on E_s and E_t to explain the reasons for the ET increase. These findings reveal the complexity of interactions between climatic factors, vegetation coverage and ET, but little attention has been paid to ET components.

A suite of ecological restoration programs have been implemented over the Loess Plateau in China to alleviate soil erosion and deforestation since 1998 (Bryan et al., 2018), making this region green in recent years (Liu et al., 2020). Moreover, this region experienced a warm-wet climate transition after 2000 (He et al., 2015). Vegetation greening and climate change likely affected the regional water-energy cycle (Feng et al., 2012; Jia et al., 2017; Wang et al., 2020; Xie et al., 2015; Zhang et al., 2019a). Many studies have explored the impact of climate change and vegetation greening on ET trends on the Loess Plateau (Bai et al., 2019; Chen et al., 2017; Gao et al., 2017; Jiang et al., 2021; Meng et al., 2020; Xie et al., 2020; Yao et al., 2019). However, these studies merely concentrated on the total water consumption, i.e., ET, rather than ET components that were the foundation for explaining the variation in ET. Although some studies have investigated the changes in ET components (Liang et al., 2020; Qiu et al., 2021; Shao et al., 2019), they did not fully explore the contributions of climatic factors and vegetation coverage to ET components, which was associated with ET partitioning after ecological restoration.

Given the importance of partitioning ET, many methods have been developed. At small scales (e.g., plot and small catchment scales), ET partitioning is generally based on observations of CO_2 and water flux variance similarity relationships, while eddy covariance-determined ecosystem-scale water use efficiency has also been used for partitioning ET (Ma et al., 2020). Moreover, transpiration and soil evaporation can be isolated either through a combination of stable isotope, sap flow, and eddy covariation techniques, or with porometer, lysimeter and Bowen ratio techniques (Lawrence et al., 2007). At large scales (e.g., watershed, regional and global scales), ET partitioning should rely on land surface models, satellite-based estimations, and relationships with groundwater (Ma et al., 2020). Land surface models generally consider biophysical processes regarding hydrological cycle, energy balance and vegetation dynamics.

This study attempted to identify the response of ET components to climate change and vegetation greening on the Loess Plateau. We employed a macroscale land-surface hydrological model, i.e., the Variable Infiltration Capacity (VIC), which well considers water constraints and energy balance, along with incorporating the remote sensing-based dynamic fractional vegetation coverage (FVC), leaf area index (LAI), albedo and shortwave/longwave radiation forcing. The aim of this study is to test the hypothesis that vegetation greening constrains soil evaporation, although it promotes vegetation transpiration. This hypothesis is expected to be helpful for understanding the hydrological effect of vegetation greenness and for evaluating water consumption in drylands with afforestation/reforestation practices.

2. Data and methods

2.1. Study area

The Loess Plateau is situated in the upper and middle reaches of the Yellow River Basin in northern China, covering an area of 632,520 km^2 and accounting for 6.3% of the entire land area of China (Fig. 1). This region includes the whole or part of seven provinces: Qinghai, Gansu, Ningxia, Inner Mongolia, Shaanxi, Henan and Shanxi. The average annual precipitation ranges from 200 mm in the northwest to 750 mm in the southeast, with 60%-70% of the rainfall occurring during summer in the form of heavy storms (Sun et al., 2015). The mean annual air temperature is 4 ℃ in the northwest and 14 ℃ in the southeast (Peng et al., 2018). Therefore, this region is a typical dryland with an arid, semi-arid and semi-humid transitional climate.

The major land cover types are grasslands and croplands, followed by forests, bare land and urban areas (Fig. 1b). After many ecological restoration programs, especially the Grain-for-Green project, had been carried out (Bryan et al., 2018), the areal coverage of grasslands and forests increased from 310,000 and 155,000 km^2 in 2001 to 370,000 and 185,000 km^2 in 2010, respectively, and correspondingly, the area of barren land and shrublands showed decreasing trends (Fan et al., 2015).

To detect the spatial variability of the vegetation greening effect, we divided the Loess Plateau into five subregions according to ecological restoration and geographic features (Yang et al., 2019), i.e., the North Loess Plateau (NLP), the Middle Loess Plateau (MLP), the East Loess Plateau (ELP), the West Loess Plateau (WLP) and the South Loess Plateau (SLP) (Fig. 1b). The NLP is a typical semi-arid area with average annual precipitation below 300 mm, mostly covered by deserts such as Mu Us Sandyland. The MLP is the central focus of vegetation restoration programs, with LAI rising by 48.4%; however, it is characterized by loess hill and gully terrains. The ELP and WLP feature rocky mountains and loess sorghum gullies, respectively. The SLP, mainly river fault depression valleys, is an economically developed area with a higher level of urbanization.

2.2. Data availability

The VIC model required various input data, including meteorological forcing, soil parameters, vegetation parameters, land cover type and topography. The meteorological forcing data consisted of daily precipitation, maximum and minimum air temperature, wind speed and relative humidity from 1990 to 2018. These gridded data, with a spatial resolution of 0.0625°, were generated by using the inverse distance weighting method to interpolate ground-based observations from 303 stations that were available from China Meteorological Administration (CMA, https://data.cma.cn/). Data of soil and vegetation parameters (e.g., architectural resistance, minimum stomatal resistance, and vegetation roughness) for each land use type were obtained from the VIC homepage (https://vic.readthedocs.io/en/master/Datasets/Datasets/) and they were generated by Nijssen et al. (2001) and successfully used in Meng et al. (2020) and Zhu et al. (2021). The land cover type data were produced by Landsat TM images at a spatial resolution of 1 km (Liu et al., 2010), obtained from National Earth System Science Data Center (https://www.geodata.cn/). It was assumed that in this study, the land cover type for 2010 was in a steady state after ecological restoration programs, as the land cover type changed little relative to the total area of the Loess Plateau during the study period (Jiang et al., 2021). Topographic data, i.e., Digital Elevation Model (DEM), were used to extract watersheds and river networks over the Loess Plateau, and were obtained from USGS (https://earthexplorer.usgs.gov/).

Remote sensing products, including downward shortwave and longwave radiation, albedo, leaf area index (LAI) and fractional vegetation cover (FVC), were also employed to drive the hydrological model.

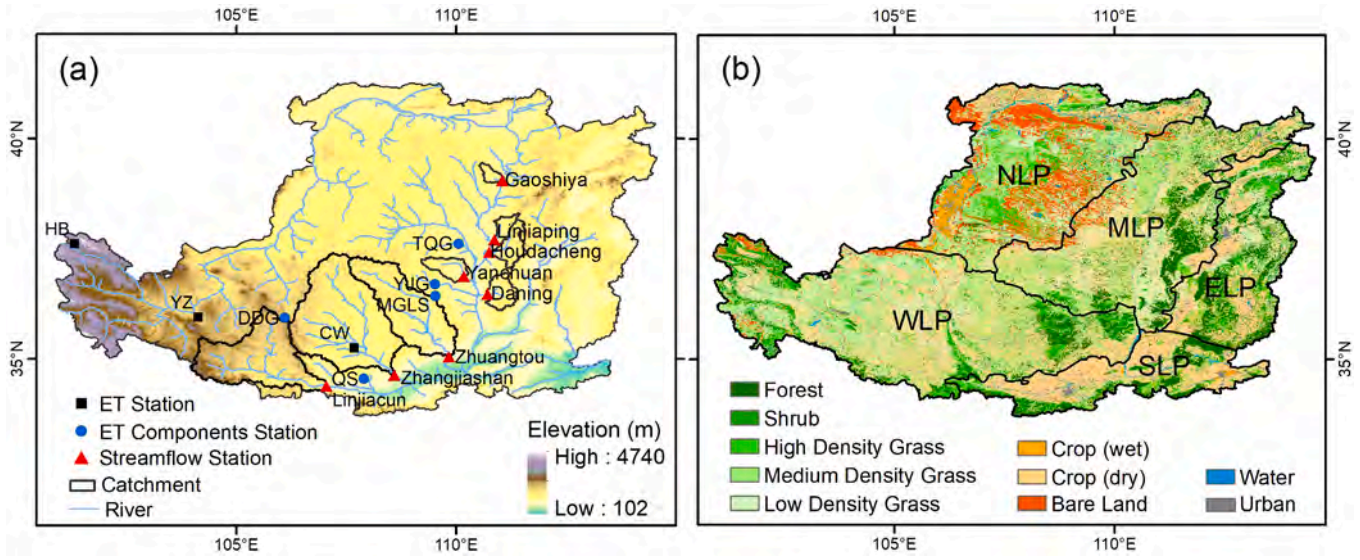

Fig. 1. (a) Location of the Loess Plateau (LP), the sites of ground-based observations of ET components, and catchments with water discharge observations; and (b) land cover distribution in the five subregions.

Apart from downward longwave radiation product which was obtained from National Tibetan Plateau Third Pole Environment Data Center (https://data.tpdc.ac.cn/zh-hans/), the other products were all derived from Global LAnd Surface Satellite (GLASS) product suite (https://www.geodata.cn/) (Liang et al., 2021; Liang et al., 2013). Downward longwave radiation product was estimated directly from temperature, surface pressure, specific humidity and downward shortwave radiation data (He et al., 2020; Yang et al., 2010). The GLASS downward shortwave radiation product was produced by using a direct estimation method based on the top atmosphere spectral reflectance of MODIS (Zhang et al., 2014). The GLASS albedo product was made by using an angular bin algorithm together with a statistics-based temporal filter algorithm (Liu et al., 2013). The GLASS LAI product (V5) was retrieved from the MODIS reflectance data using the general regression neural networks algorithm (Xiao et al., 2014) and it was updated using a deep learning model (Ma and Liang, 2022). The GLASS FVC product was also obtained by using the general regression neural networks algorithm based on Landsat TM/ETM + and MODIS reflectance data (Jia et al., 2015). To adapt to simulations with the VIC model, the 8-day composite LAI and FVC data were linearly interpolated to a daily resolution.

To evaluate the model performance for ET and its components, several types of data, including ground-based observations, water balance-derived estimates and remote sensing retrievals, were implemented. We collected ground-based daily ET observations from three covariance flux towers (Fig. 1a and Table 1) of the Coordinated Enhanced Observation Project in arid and semi-arid regions in northern China. The ET component data from field experiments were also obtained to validate E_c, E_t, and E_s, and these data have been successfully used to detect the water consumption from vegetation and bare soil, as evidenced in the literature listed in Table 2. Please note the measurements of ET, E_c, E_t and E_s located different sites, and their data were at different time scales (i.e., daily scales for ET and monthly scales for the three components).

The ground-based observations of total ET and its components only represent small-scale evaporation flux (<1 km^2); therefore, we derived annual water balance-based ET estimates, i.e., $ET = P - Q - \Delta S$, where P is the annual precipitation, Q is the annual runoff, and ΔS is the change of total water storage. The annual runoff was calculated based on monthly streamflow data of eight catchments on the Loess Plateau (Fig. 1a), which were obtained from the Annual Hydrological Report for China. The change of total water storage (ΔS) of each catchment was derived from the Gravity Recovery and Climate Experiment (GRACE) with respect to the average of three solutions, i.e., CSR (https://www2.csr.utexas.edu/grace/), GSFC (https://earth.gsfc.nasa.gov/geo/) and JPL Mascon (https://grace.jpl.nasa.gov/).

Moreover, we collected two remote sensing ET products from Global Land Evaporation Amsterdam Model (GLEAM) (Martens et al., 2017; Miralles et al., 2011) and Penman-Monteith-Leuning (PML) (Zhang et al., 2019b; Zhang et al., 2016b). Both the GLEAM and PML products used LAI to represent vegetation dynamics and simply considered water balance. GLEAM ET was at 0.25° and daily resolution and PML ET was at 0.05° and 8-day resolution, both of which were interpolated to 0.0625° and daily resolution in this study. To relieve their uncertainties, we averaged the two products to obtain a more reliable ET estimation, which was referred to as remote sensing ET in this study.

Table 1
Basic information for ET observations.

Flux tower	Lat, Lon	Year (month)	Vegetation type
Haibei (HB)	37.62°, 101.32°	2002–2004 (1–12)	Shrub
Yuzhong (YZ)	35.95°, 104.13°	2008–2009 (7–9)	Grass
Changwu (CW)	35.25°, 107.68°	2008–2009 (7–9)	Grass

2.3. Hydrological model for ET partitioning

The Variable Infiltration Capacity (VIC) model was adopted to estimate ET components and to detect their drivers on the Loess Plateau. The VIC model, an extensively used macroscale hydrological model (Liang et al., 1994; Liang et al., 1996), is able to solve the problems of water and energy balance with vegetation, soil and atmosphere (Haddeland et al., 2006; Nijssen et al., 2001; Painter et al., 2010). It is a grid-based model that can be implemented at different spatial (from 0.0625° to 2° latitude by longitude) and temporal resolutions (from hourly to daily). For land cover variability, each grid cell is partitioned into multiple vegetation types and bare soil, and the soil column is typically divided into three (or more) layers, so the model considers root distribution in multiple layers, but it fails to represent growth with root dynamics; however, it can incorporate remote sensing products (e.g., LAI and FVC) to partly remedy this issue. Hydrological states and variables, such as infiltration, surface runoff, subsurface runoff, evapotranspiration (ET), land surface temperature and energy flux, are calculated at the subgrid scale and finally aggregated to the grid scale.

We briefly describe the formulation of the ET and its components

Table 2
Basic information for ET components. The tick (√) means the data are available.

Station	Lat., Lon.	E_t	E_s	E_c	Year (month)	Method	Vegetation type	Reference
Yangjuangou (YJG)	36.70°, 109.52°	√	√	√	2013–2014 (5–9) 2015–2016 (6–9)	Sap flow, Microlysimeter	Black locust	Jiao et al. (2016)Jiao et al. (2018)
Mt Gonglushan (MGLS)	36.42°, 109.53°	√			2008–2010 (4–10)	Sap flow	Black locust	Zhang et al. (2015a)
Qishui (QS)	34.55°, 107.90°	√			2015 (6–9) 2016 (5–9)	Sap flow	Black locust	Zhang et al. (2018)
Tuqiaogou (TQG)	37.62°, 110.05°	√	√	√	2003–2004 (5–10)	Microlysimeter, Portable photosynthesis system	Black locust, Platycladus orientalis	Tian (2005)
Diediegou (DDG)	35.97°, 106.15°	√			2006 (6–9)	Water balance, Thermal dissipation probes, Microlysimeter, Pluviometer	Larch	Liu (2008)

here. The VIC model partitions ET into four components: soil evaporation (E_s), vegetation transpiration (E_t), canopy interception loss (E_c) and snow sublimation (E_{sn}). The total ET over a grid cell is computed as the sum of the above components, weighted by their respective surface cover area fractions, which is:

$$ET = \sum_{n=1}^{N} C_n \cdot (E_{c,n} + E_{t,n}) + C_{N+1} \cdot E_s + E_{sn} \quad (1)$$

where C_n is the fractional vegetation coverage (FVC) for the nth vegetation title, which is often regarded as a constant in the study period, but a dynamic FVC can better represent vegetation growth, providing more accurate ET simulations. C_{N+1} is the soil fraction, and $\sum_{n=1}^{N+1} C_n = 1$.

Vegetation transpiration, canopy interception loss and soil evaporation are all developed by constraining the potential evapotranspiration from the Penman–Monteith formulation (Shuttleworth, 1993), which sets the bulk surface resistant as zero to be simplified to the Penman formulation for potential ET computation in this model:

$$E_p = \frac{\Delta(R_n - G) + \rho_a C_p D / r_a}{\lambda(\Delta + \gamma)} \quad (2)$$

where E_p is the potential evapotranspiration (mm day^{-1}), R_n is the net radiation (W m^{-2}), G is the ground heat flux (W m^{-2}), D is the vapor pressure deficit (VPD) of the air (Pa), ρ_a is the density of air at constant pressure (kg m^{-3}), C_p is the specific heat of the air (J kg^{-1} K^{-1}), r_a is the aerodynamic resistance (s m^{-1}), λ is the latent heat of vaporization (J kg^{-1}), Δ is the slope of the saturation vapor pressure curve at the temperature of interest (Pa K^{-1}) which is a function of temperature, and γ is the psychrometric constant (Pa K^{-1}).

For the area with vegetation coverage, canopy interception loss is calculated as a fraction of the potential ET,

$$E_c = f \cdot \left(\frac{W_i}{W_{im}}\right)^{2/3} E_p \frac{r_a}{r_a + r_o} \quad (3)$$

where E_c is the canopy interception loss (mm), f is the fraction of the time step when canopy interception loss happens, r_o is the architectural resistance (s m^{-1}), W_i is the amount of water the canopy intercepts (mm), and W_{im} is the maximum amount of water that the canopy can intercept (mm), which is parameterized to be proportional to the LAI.

After canopy interception loss, vegetation transpiration can occur and is estimated as:

$$E_t = (1 - f) E_p \frac{r_a}{r_a + r_o + r_c} + f \cdot \left(1 - \left(\frac{W_i}{W_{im}}\right)^{2/3}\right) E_p \frac{r_a}{r_a + r_o + r_c} \quad (4)$$

where E_t is vegetation transpiration (mm), and r_c is the canopy resistance (s m^{-1}) expressed as:

$$r_c = \frac{r_{0c} g_T g_{vpd} g_{PAR} g_{sm}}{LAI} \quad (5)$$

where r_{0c} is the minimum canopy resistance (s m^{-1}); g_T, g_{vpd}, and g_{PAR} are the temperature factor, VPD factor, and photosynthetically active radiation flux (PAR) factor, respectively; g_{sm} is a soil moisture stress factor that depends on the soil moisture content; and *LAI* is the leaf area index (m^2 m^{-2}), which is usually a static (interannually invariant) index in most studies, but dynamic LAI is used to reflect the interannual change in vegetation in this study.

Soil evaporation only occurs for the area without vegetation coverage (i.e., bare land) on the top thin layer. When the surface soil is saturated, it evaporates at the potential evaporation rate; otherwise, its evaporation varies according to the heterogeneities in infiltration, topography and soil characteristics. Soil evaporation is described as:

$$E_s = E_p \left(\int_0^{A_s} dA + \int_{A_s}^{1} \frac{i_0}{i_m (1 - (1 - A)^{1/b_i})} dA \right) \quad (6)$$

where E_s is the soil evaporation (mm), i_m is the maximum infiltration capacity (mm), A is the fraction of area for which the infiltration capacity is less than the current infiltration capacity i, b_i is the infiltration shape parameter, A_s represents the fraction of the bare soil that is saturated, and i_0 represents the corresponding point infiltration capacity. So E_s is dependent on soil moisture condition.

Snow sublimation is calculated directly from a modified energy balance. Energy exchange between atmosphere, forest canopy and snowpack occurs only within the surface layer. For specific calculations of the snow sublimation, and the parameters and variables described above, please refer to the original VIC papers (Liang et al., 1994).

From the above description, we can see that the VIC model features prominently in the computation of the ET components by considering energy balance and establishing water constraints, so that the interaction between soil moisture dynamics and ET processes are well formulated. This feature makes it more suitable for ET estimation than remote sensing-based ET algorithms in water-limited conditions, which generally only employ energy balance to constrain, e.g., the Priestley–Taylor Jet Propulsion Laboratory (PT-JPL) model (Fisher et al., 2008). As expressed in the above equations, the VIC model also applies vegetation structure (i.e., LAI for each land use type) and coverage (i.e., FVC) to reflect the impact of land cover on ET. However, the original version of the VIC generally employs static LAI and FVC with climatological conditions, which is able to represent seasonal variability rather than interannual dynamics. To remedy this issue, this study applied daily LAI and FVC from the GLASS products to force the VIC simulations, and this application has been demonstrated to be effective in hydrological simulations due to the representation of vegetation dynamics (Jiang et al., 2021; Meng et al., 2020).

2.4. Simulation experimental design

We designed one baseline and three detrended scenarios, i.e., P-det, V-det and Ra-det (Table 3), to quantify the hydrological effects of precipitation change, vegetation greening and radiation change, respectively, on the Loess Plateau for 2000–2018. The four were run at

Table 3
Simulation scenarios used to detect the contribution of precipitation, vegetation and radiation (longwave radiation R_l and shortwave radiation R_s) during 2000–2018.

Scenarios	Precipitation	LAI	FVC	albedo	R_l	R_s
Baseline	Real	Real	Real	Real	Real	Real
P-det	Detrended	Real	Real	Real	Real	Real
V-det	Real	Detrended	Detrended	Detrended	Real	Real
Ra-det	Real	Real	Real	Real	Detrended	Detrended

spatial–temporal resolutions of 0.0625° and 3 h to achieve water and energy balances. The difference in ET and its components between the baseline scenario and the different detrended scenario is assumed to represent the contributions of precipitation change, vegetation greening or radiation change. For the baseline scenario, the model was run using the original forcing data, including dynamic vegetation coverage and radiation forcing. For the P-det scenario, the trend of precipitation was linearly removed, and the other forcing variables remained the same as those in the baseline scenario. Similarly, with respect to the Ra-det scenario, the downward longwave and shortwave radiation data were linearly detrended. The detrended method used in the P-det and Ra-det simulation schemes is as follows:

$$V'_{Y_{i,d}} = \left(\frac{V_{Y_i} + a\cdot(Y_b - Y_i)}{V_{Y_i}}\right)\cdot V_{Y_{i,d}} \quad (7)$$

where Y_i is a year within 2000–2018; $V'_{Y_{i,d}}$ is the detrended daily precipitation, shortwave radiation or longwave radiation on day d in the year Y_i; $V_{Y_{i,d}}$ is the original daily precipitation, shortwave radiation or longwave radiation; V_{Y_i} is the annual daily precipitation, shortwave radiation or longwave radiation in the year Y_i; Y_b is the reference year, 2000; and a is the linear trend of annual precipitation, shortwave radiation or longwave radiation. The detrended time series ($V'_{Y_{i,d}}$) maintains the seasonal variations but has no interannual trend.

For the V-det scenario, the daily mean values of LAI, FVC and albedo during 2000–2002 were used to drive the VIC model for the period 2000–2018. This strategy not only removes the variation trend but also avoids abrupt land cover changes in a given year. While there are many factors influencing land surface albedo (e.g., vegetation coverage, soil moisture, and snow coverage), land use and land cover are generally assumed as the primary factors. Therefore, this study takes the effect of albedo on ET as one of the vegetation contributors, although it is connected to radiation balance.

3. Results

3.1. Model evaluation

3.1.1. Ground-based evaluation

The metrics of root mean square error (RMSE), Pearson correlation coefficient (R), and the relative bias (*Bias*) were used to examine the robustness of the VIC model. We first compared simulations with ground-based observations. Fig. 2 shows the simulated ET against observed ET at three towers on a daily basis. The simulated ET is consistent with the observations as the R is up to 0.68 and the relative bias ranges from − 35.4% to − 2.7%. The model also presents acceptable performance for transpiration (E_t), canopy interception loss (E_c) and soil evaporation (E_s) simulations. The R for E_t is more than 0.45 with the relative bias < 24.8% (Fig. 3). Similar levels of the three metrics are obtained for E_c and E_s, while the numbers of their observation points are relatively small (Fig. 4).

The VIC model was further evaluated based on the catchment-scale runoff and the associated water balance-derived ET. We used another metric, i.e., the Kling–Gupta efficiency index (KGE) (Gupta et al., 2009), instead of RMSE to detect the runoff simulation performance, as it is more robust and widely used in streamflow evaluation (Althoff and Rodrigues, 2021). As shown in Table 4, the model can reasonably simulate the monthly runoff for the eight catchments with KGE more than 0.31 and *Bias* < 33.93%. The simulations generally capture the peak flow and baseflow well at most stations, although relatively poor performance occurs when tracing the peak flow at Linjiaping and Gaoshiya stations (Fig. 5). For the water balance-derived ET, the model achieves R of 0.69 and *Bias* of − 5.2% (Fig. 5i). Although the model seems to slightly underestimate ET and the components to some degree,

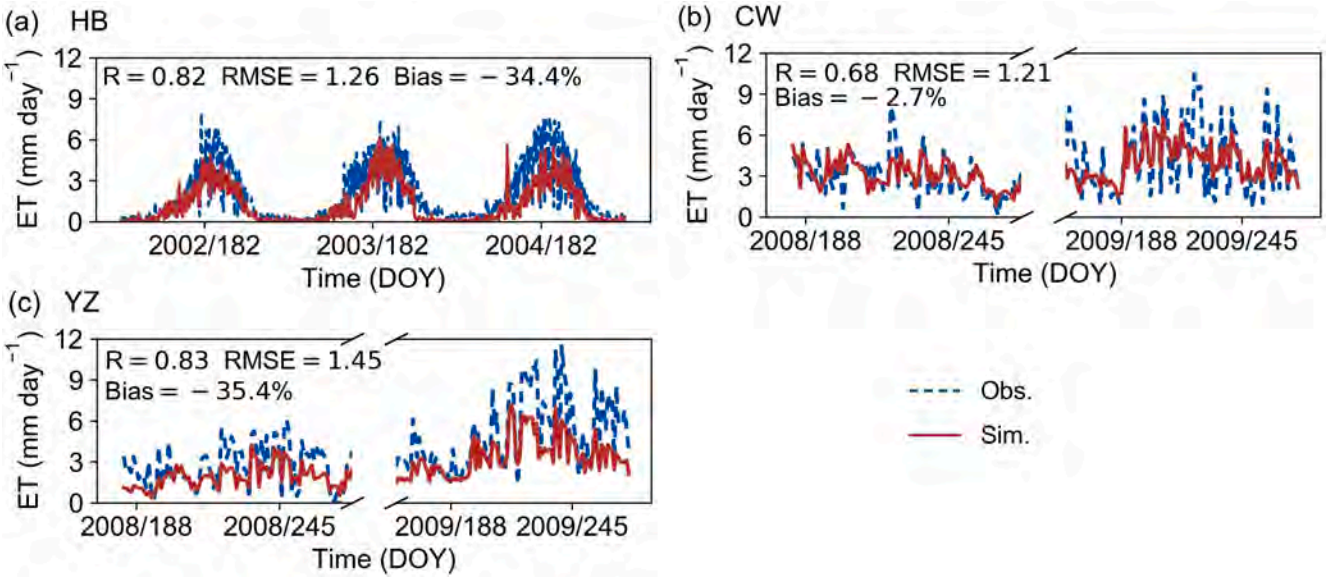

Fig. 2. Simulated daily ET against observed ET at three covariance flux towers on a daily basis: (a) HB Station, (b) CW Station, (c) YZ Station. The sites of the three towers are shown in Table 1.

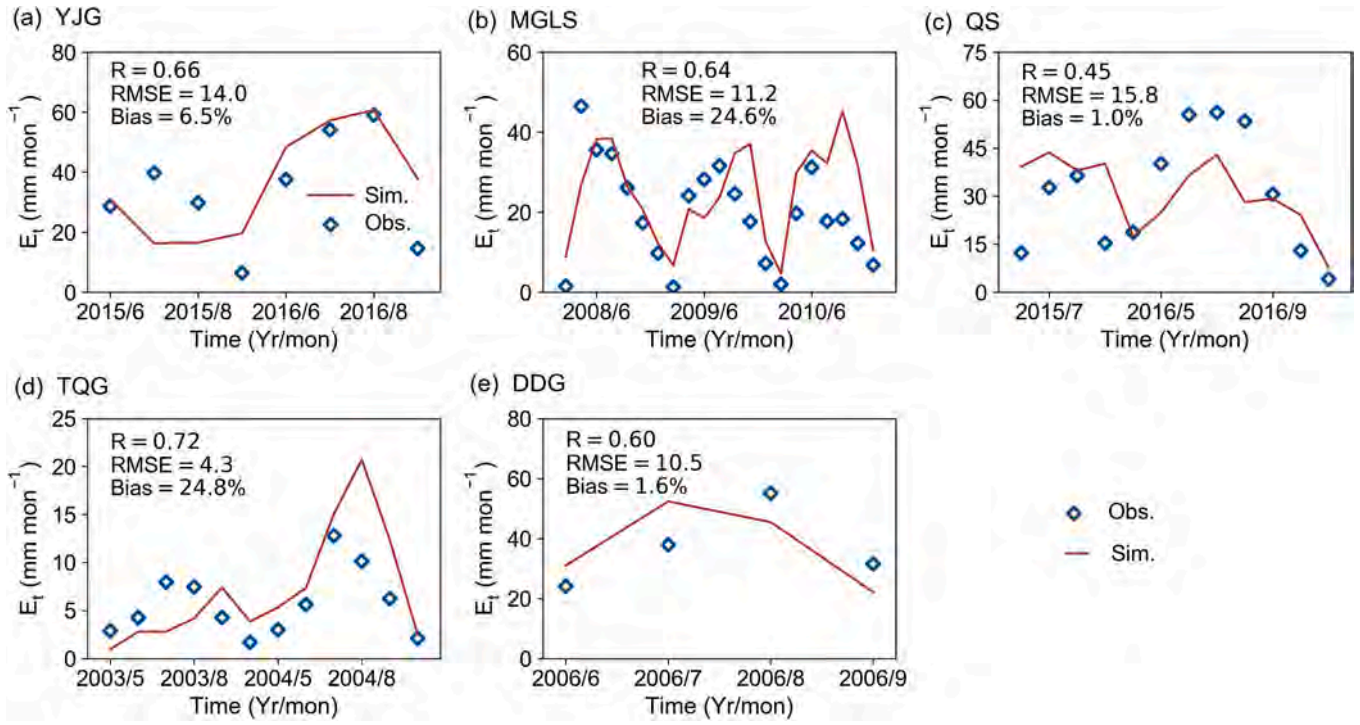

Fig. 3. Simulated E_t against observed E_t on a monthly basis for five stations: (a) YJG, (b) MGLS, (c) QS, (d) TQG, and (e) DDG. The sites of the five stations are shown in Table 2.

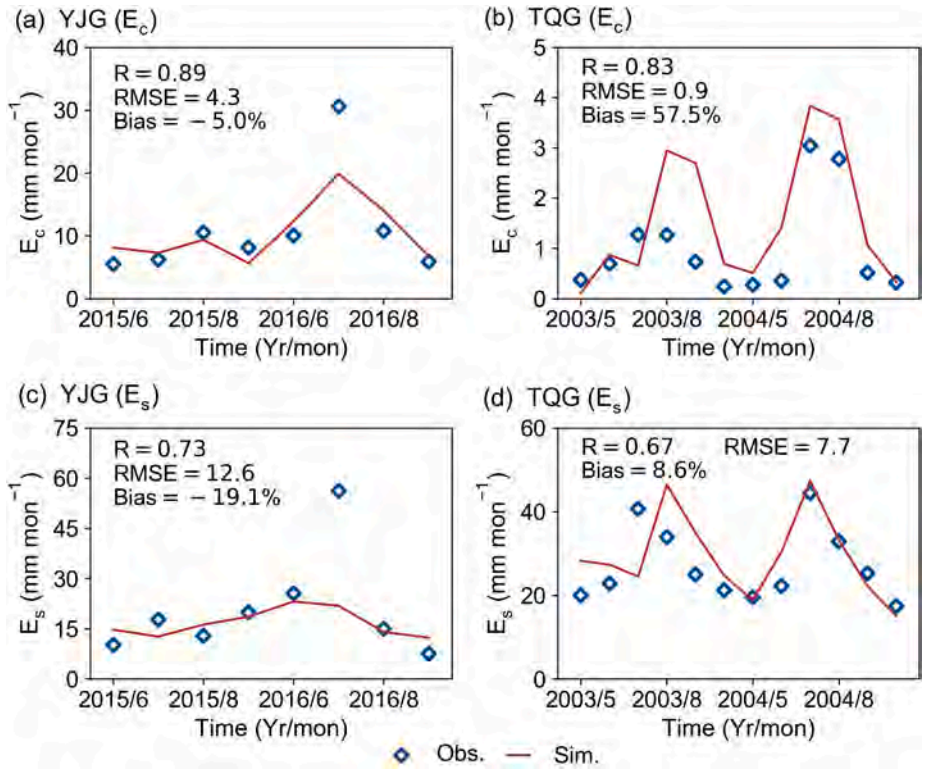

Fig. 4. Simulated E_c and E_s against observed E_c and E_s on a monthly basis: (a) E_c at YJG Station, (b) E_c at TQG Station, (c) E_s at YJG Station, (d) E_s at TQG Station. The sites of the two stations are shown in Table 2.

the overall performance is acceptable to match the ground-based observations.

3.1.2. Remote sensing-based comparison

In addition to the ground-based evaluation, we employed GLEAM and PML products, both of which simply incorporated water constraints by solving the water balance equation with precipitation as input in the

Table 4
Model performance for the eight catchments.

Station	Calibration			Validation		
	KGE	R	Bias (%)	KGE	R	Bias (%)
Yanchuan	0.74	0.89	20.09	0.40	0.94	33.93
Daning	0.83	0.84	5.33	0.66	0.89	11.72
Linjiaping	0.47	0.57	−5.70	0.45	0.65	−15.48
Houdacheng	0.62	0.65	16.48	0.58	0.80	23.62
Gaoshiya	0.31	0.70	−28.16	0.61	0.67	13.40
Zhuangtou	0.56	0.82	−32.31	0.55	0.59	7.82
Zhangjiashan	0.59	0.93	−23.52	0.70	0.77	10.77
Linjiacun	0.63	0.92	17.42	0.50	0.71	−1.53

ET estimation. Fig. 6 compares the simulated ET with remote sensing ET (i.e., the average between GLEAM ET and PML ET) in the growing season (May-October) during the period 2003–2018 since the PML product has a large amount of missing data for the first three years of 2000–2002. The spatial pattern of the simulated ET is in agreement with that of the remote sensing estimation, displaying lower values in the northwest and higher values in the southeast (Fig. 6a and b) and with *Bias* ranging between − 40% and 20% (Fig. 6c). The simulated inter-annual ET variability also closely follows that of the remote sensing ET, with *R* of 0.91 and *Bias* of − 3.40% (Fig. 6d).

To further confirm our simulations, ET and its components (E_t, E_c and E_s) of our study were compared with those of GLEAM and PML for the growing season during 2003–2018. We focused the inter-annual variations of the four variables, which was important to reflect the change trends of the four. Thus, we computed their time series anomalies by removing their long-term means. The trends of the four components from the three estimations are consistent: ET, E_t, and E_c increase but E_s decreases in this period despite slight differences between the VIC simulation and the other two products (Fig. 7). This consistency also indicates the reliability of the estimations of the ET components.

3.2. Spatial distribution

The spatial distribution of the mean annual ET and the ratio of each ET component are shown in Fig. 8. The mean annual ET over the entire region is about 390 mm, but large spatial heterogeneity can be seen in the study area, with lower values (<200 mm) in the northwestern part and higher values (greater than 500 mm) in the southeastern part (Fig. 8a). This spatial pattern is consistent with the distribution of precipitation. Averaged over the whole region, E_s accounts for the largest proportion of ET, about 60%, followed by E_t, E_c and E_{sn} (Fig. 8b), which indicates that soil evaporation consumes more water than vegetation transpiration. However, the ratios of the four components to the total ET present contrasting spatial distributions (Fig. 8c-f). In the NLP and northern part of the WLP, ET primarily comes from E_s with E_s/ET above 75% because the land cover type is mainly desert and these areas are under a dry climate. In contrast, in the ELP, and eastern part of the WLP and MLP, E_t is the main contributor with E_t/ET greater than 50%, and E_c/ET is also as high as 15%, because the land cover in these areas is dominated by forest and grassland. In terms of E_{sn}, it occupies only a little portion of ET, below 6%, except for a small area in the western part of the WLP whose elevation is more than 4000 m.

3.3. Temporal changes

To detect the difference of the changes in ET and its components, so as to identify which one is the largest contributor to the total ET,

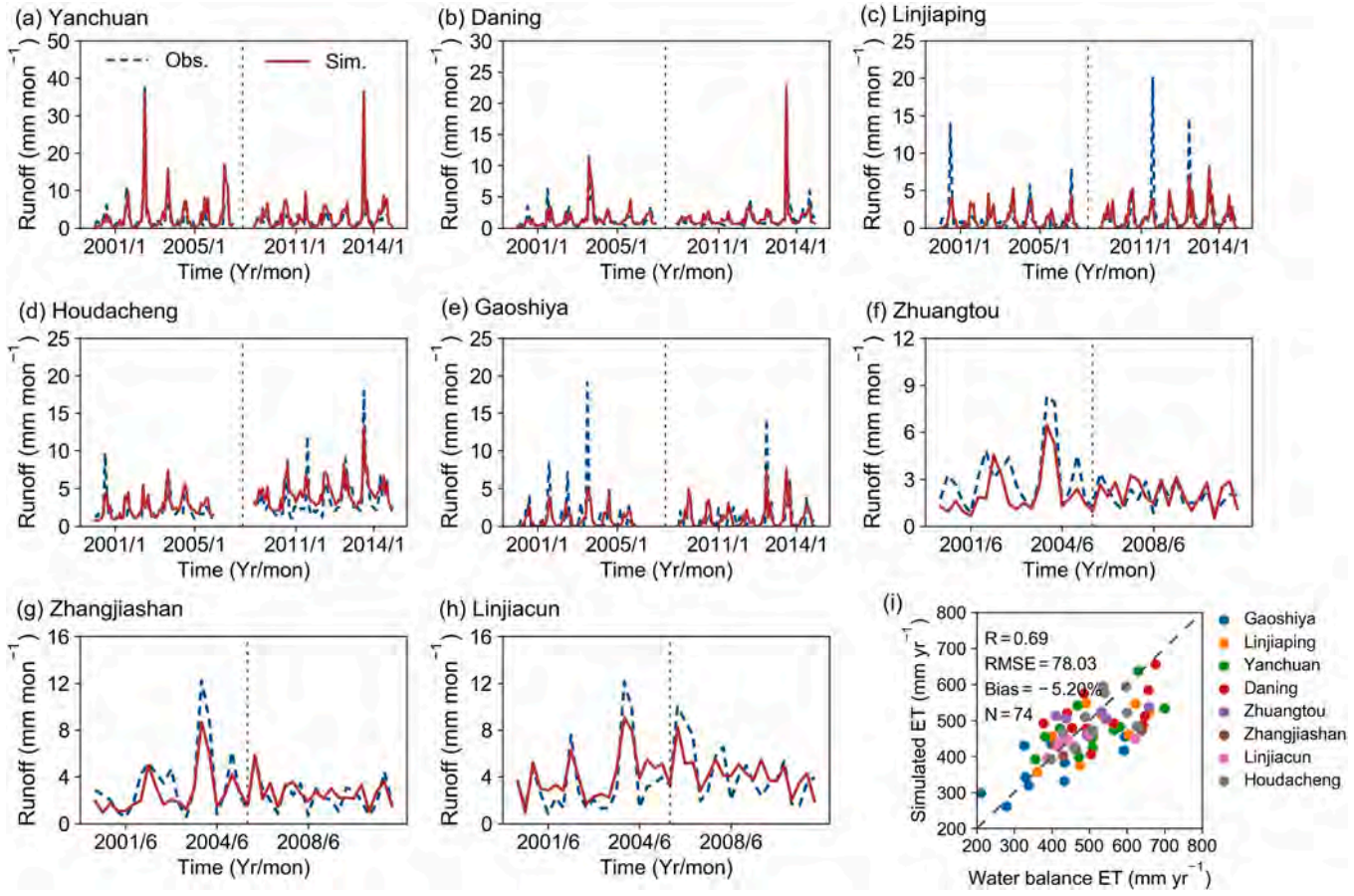

Fig. 5. Simulated runoff against observed runoff for eight catchments on a monthly basis for eight stations: (a) Yanchuan, (b) Daning, (c) Linjiaping, (d) Houdacheng, (e) Gaoshiya, (f) Zhuangtou, (g) Zhangjiashan, and (h) Linjiacun. (i) Comparison of the simulated ET to water balance ET at annual scale for the eight catchments.

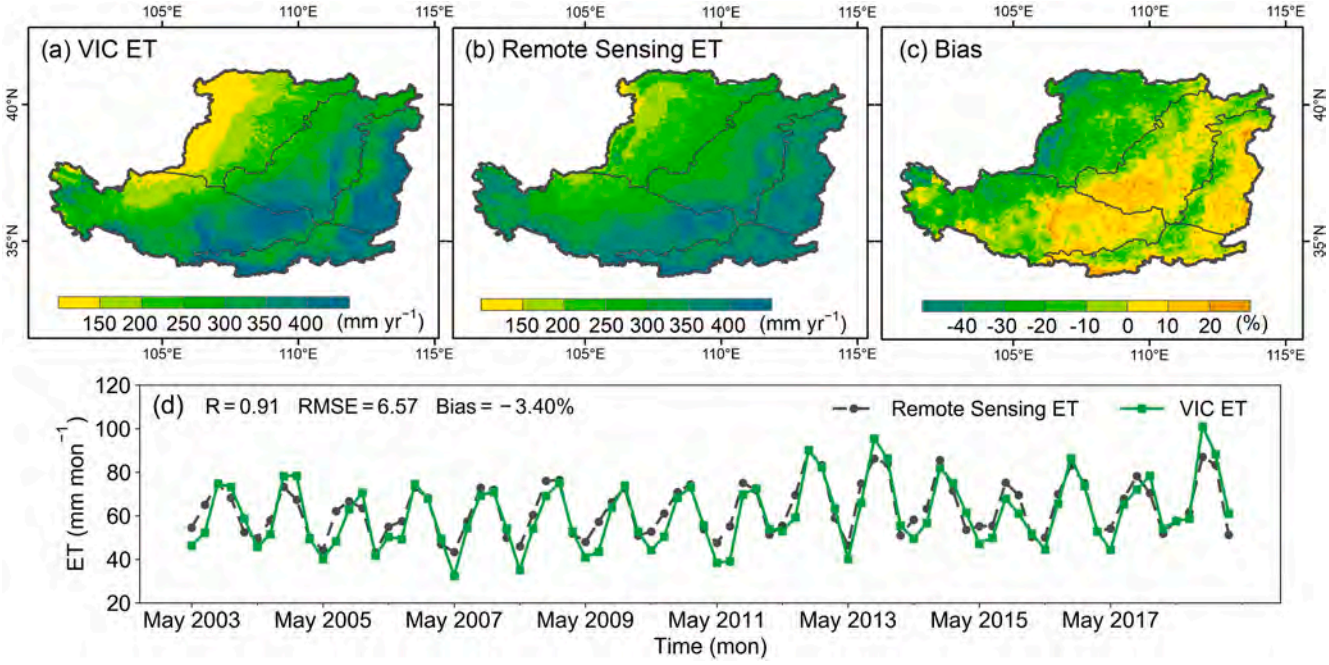

Fig. 6. Total ET in the growing season (May-October) obtained from VIC and the remote sensing data (the average between GLEAM ET and PML ET) over the period of 2003–2018: (a) mean VIC ET; (b) mean remote sensing ET; (c) Bias between the VIC ET and the remote sensing ET; and (d) monthly time series of VIC ET and the remote sensing ET.

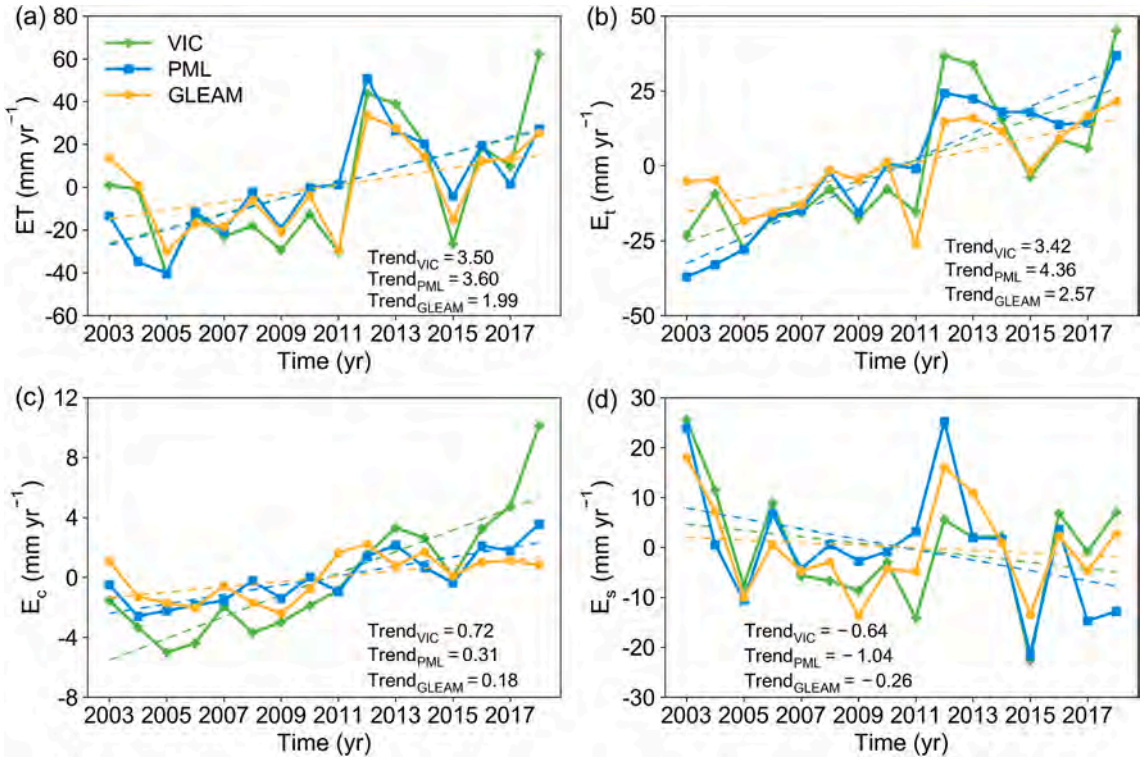

Fig. 7. Comparisons of mean annual ET and its components from VIC, PML and GLEAM in the growing season during 2003–2018: (a) ET, (b) transpiration (E_t), (c) canopy interception loss (E_c), and (d) soil evaporation (E_s).

interannual variations are depicted in Fig. 9a. The average annual ET on the Loess Plateau exhibits a significantly increasing trend of 5.73 mm yr^{-1}, totalling 108.87 mm during 2000–2018, which results from the significant positive trends in E_t (4.76 mm yr^{-1}, $P < 0.01$) and E_c (0.91 mm yr^{-1}, $P < 0.01$), while the trends of E_s (0.09 mm yr^{-1}) and E_{sn} (−0.03 mm yr^{-1}) are relatively small. Fig. 9b presents the temporal variation in the ratios of ET components to ET. Despite the slight increase in E_s, the ratio of E_s (E_s/ET) shows a significant downward trend of − 7.67% decade^{-1}, which means it decreases from 61.80% in 2000 to 44.85% in 2018. In contrast, E_t/ET and E_c/ET rise significantly with

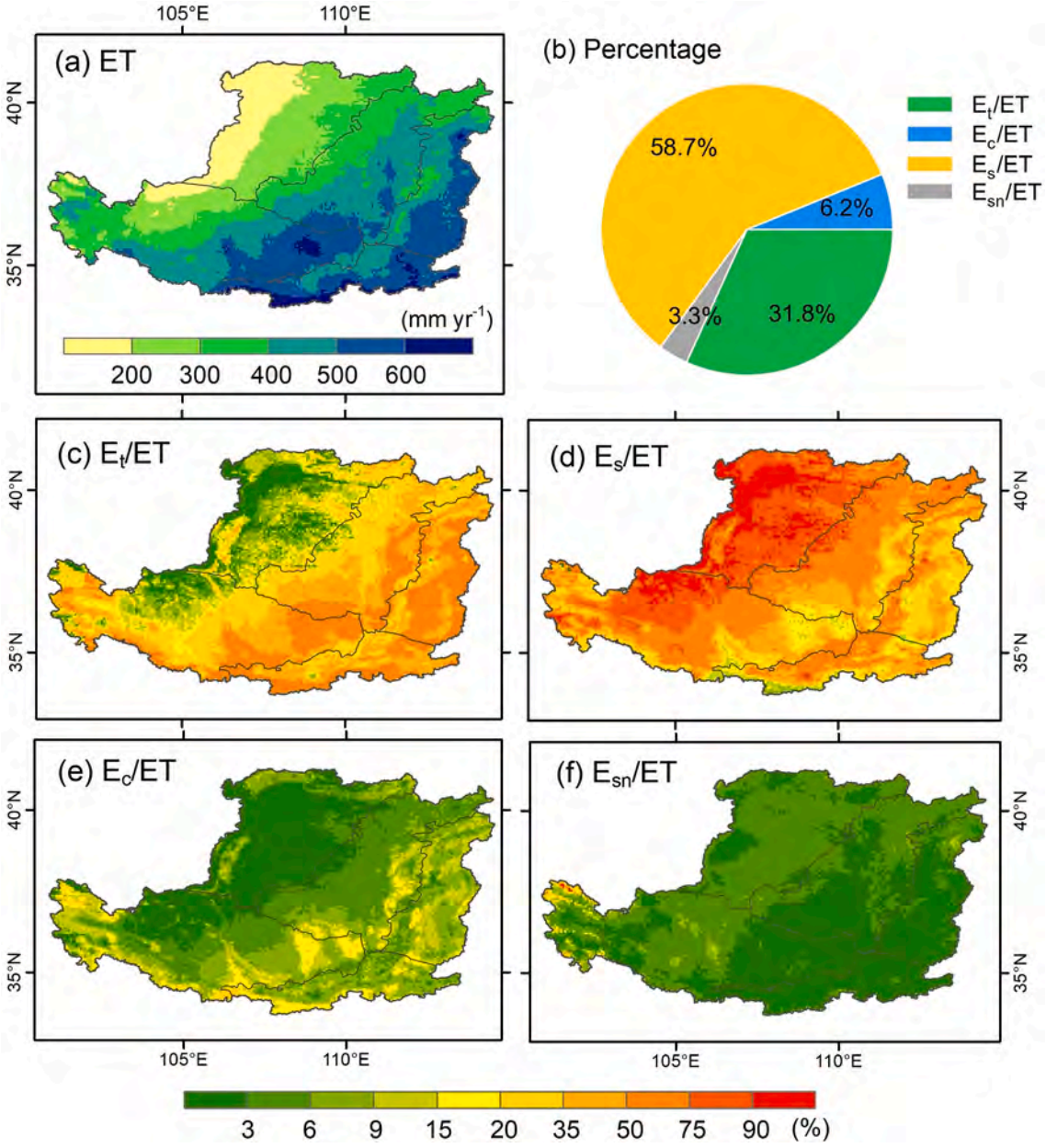

Fig. 8. Spatial distributions of ET and its components on the Loess Plateau during 2000–2018: (a) mean annual ET; (b) the ratio of ET components averaged over the whole region; (c) the ratio of transpiration (E_t) to ET; (d) the ratio of soil evaporation (E_s) to ET; (e) the ratio of canopy interception loss (E_c) to ET; and (f) the ratio of snow sublimation (E_{sn}) to ET.

rates of 6.92% decade^{-1} (from 28.04% to 43.81%) and 1.27% decade^{-1} (from 6.05% to 8.49%), respectively, and the variation in E_{sn}/ET is negligible. Therefore, vegetation transpiration has recently become the primary component in the ET process.

The seasonal cycle of ET and the four components may change during the vegetation greening period. We analysed the difference in their seasonal cycle between the early stage (2000–2003) and the recent stage (2015–2018). The seasonal cycles at the two stages were calculated by averaging the four-year seasonal variability. As shown in Fig. 10a and b, the recent stage E_t and E_s are quite distinct from the early stage. Specifically, E_t is smaller than E_s during the yearly cycle at the early stage, but this pattern changes at the recent stage as E_t overtakes E_s during the warm season (from June to September). In the warm season, the difference in E_t is over 10 mm mon^{-1}, while the difference in E_s is about − 5 mm mon^{-1} (Fig. 10c). The differences in this season represent a 10% increase in E_t and a 15% decrease in E_s. ET rises for all months, especially in July and August which is contributed by the substantial increase in E_t. Snow sublimation (E_{sn}) primarily occurs in winter with 2.09 mm mon^{-1}, occupying a large portion (33.13%) of the total ET. Moreover, the phenology of the peak values of E_t, E_s and ET advances from August at the early stage to July at the recent stage (Fig. 10a and b).

3.4. Contributions analysis

3.4.1. Changes in precipitation, vegetation and radiation

Before quantifying the contributions of precipitation, vegetation and radiation to ET and its components, we first identified the variations in these factors. As shown in Fig. 11, the area with increased precipitation occupies 94% of the Loess Plateau, 18% of which significantly increases, and the maximum (>10 mm yr^{-1}) is mainly distributed in the MLP, and decreased precipitation is sporadically distributed in the southeastern Loess Plateau (Fig. 11a). Overall, precipitation has a significant increase

Fig. 9. (a) Temporal variations in ET and its components and (b) their ratios over the period 2000–2018. The asterisk (**) denotes statistical significance at $P < 0.01$.

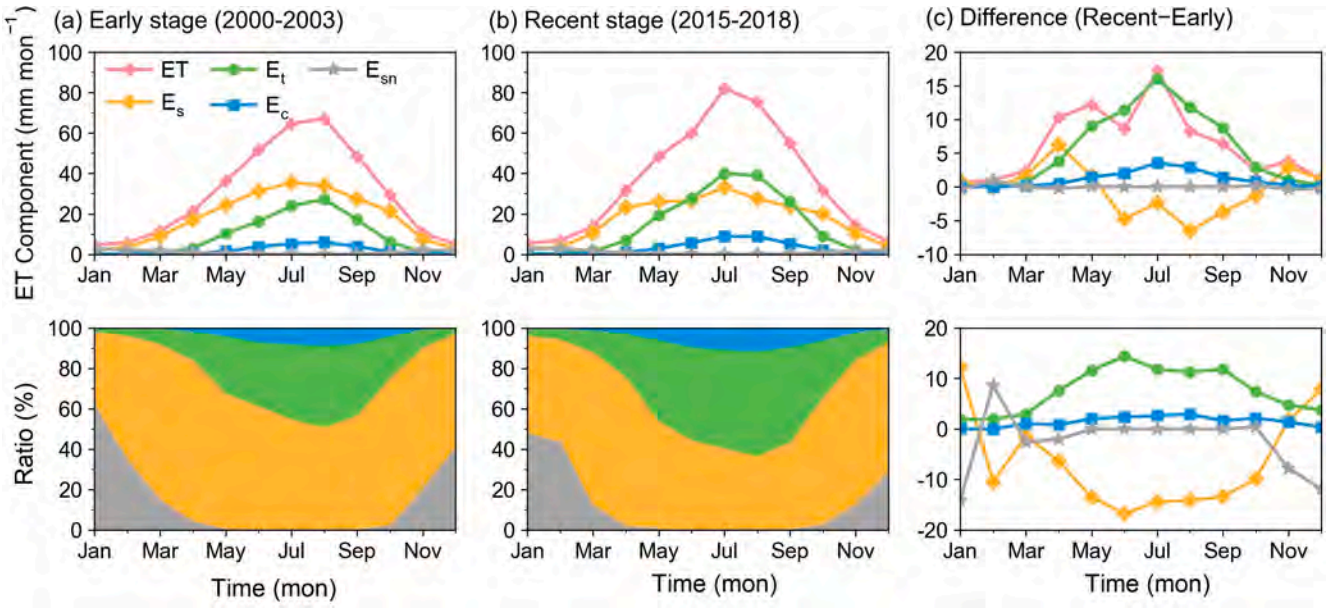

Fig. 10. Seasonal cycle of ET and its components and their ratios in two stages: (a) early stage (2000–2003), (b) recent stage (2015–2018), and (c) difference between the two stages, i.e., the ET and its components at the recent stage minus them at the early stage.

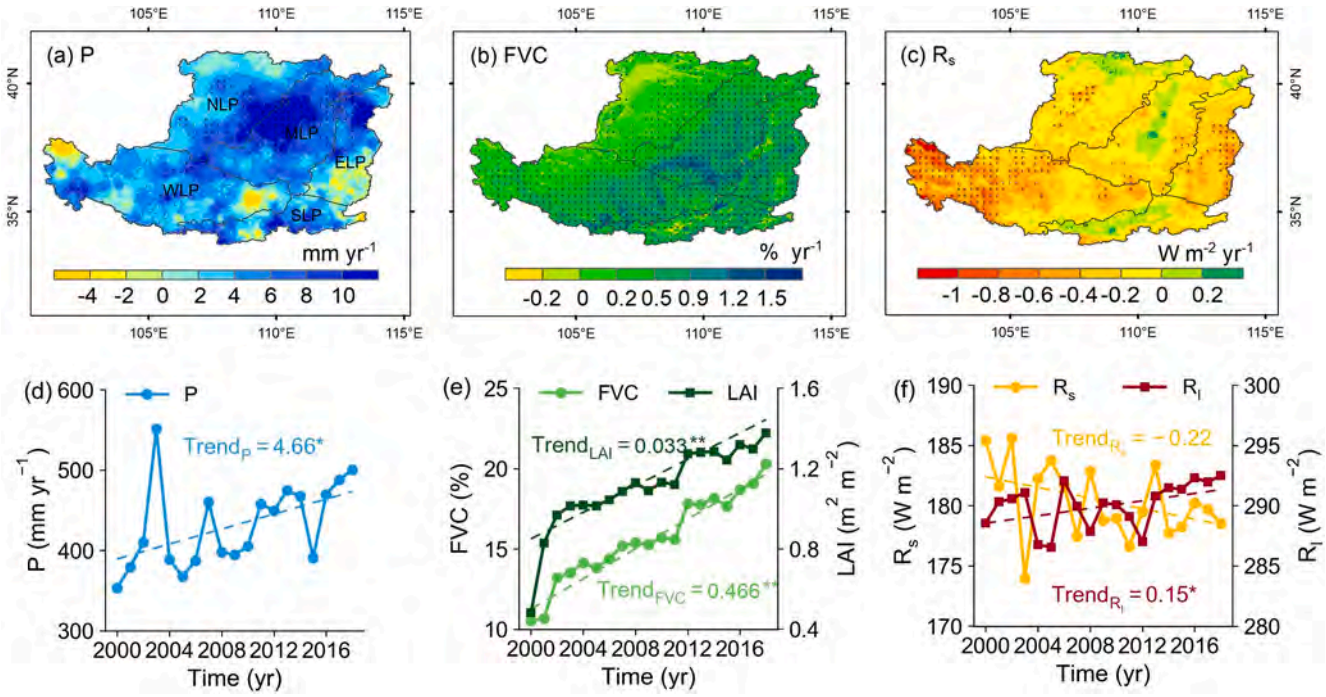

Fig. 11. Trends of (a) precipitation, (b) FVC and (c) shortwave radiation (R_s); time series of (d) precipitation, (e) FVC and LAI, and (f) shortwave/longwave radiation during 2000–2018. The black cross (+) in (a)-(c) denotes statistical significance at $P < 0.05$. The asterisks (** and *) in (d)-(f) denote statistical significance at $P < 0.01$ and $P < 0.05$, respectively.

with a rate of 4.66 mm yr^{-1} ($P < 0.05$) for the period of 2000–2018 (Fig. 11d). Similarly, FVC rises in 92.0% of the whole region, with 87.6% of the area having significant increases and the highest positive trends reaching 1.5% yr^{-1} (Fig. 11b). Averaged over the Loess Plateau, both FVC and LAI exhibit upward trends at 0.466% yr^{-1} ($P < 0.01$) and 0.033 $m2/m^{-2}$ yr^{-1} ($P < 0.01$), but they are only 20% and 1.3 $m2/m^{-2}$ in 2018, respectively, which may imply the limited vegetation transpiration (Fig. 11e). However, the area with shortwave radiation decreasing accounts for 88.7% of the study region, especially in the western part of the WLP, whose values are up to −0.8 W m^{-2} yr^{-1}, and the increasing rates are mostly in some parts of the NLP, MLP and SLP (Fig. 11c). Generally, shortwave radiation declines, while longwave radiation rises (Fig. 11f).

3.4.2. Yearly-scale contributions

In addition to the baseline simulation, as described in subsection 2.4, the other three detrended simulations were conducted to quantify the contributions of precipitation, vegetation and radiation to ET processes. The linear trend of the difference between each of the detrended simulations and the baseline simulation was calculated to represent the magnitude of the contribution. As shown in Fig. 12, precipitation induces annual ET increase in 75% of the study area with a magnitude of 2.87 mm yr^{-1}. This contribution results from the induced primary increases in E_s (1.42 mm yr^{-1}) and E_t (1.30 mm yr^{-1}) and the minor increases in E_c and E_{sn}. Obviously, vegetation greenness promotes E_t and E_c at rates of 3.21 mm yr^{-1} and 0.672 mm yr^{-1}, respectively, but it decreases E_s at a rate of − 2.36 mm yr^{-1}. Therefore, the contribution of vegetation greenness to ET is about 1.52 mm yr^{-1}. The effect of the radiation change on ET and its components can be ignored, ranging from − 0.05 to 0.009 mm yr^{-1}. Moreover, E_c and E_{sn}, whose ratios to ET are quite small, are mainly affected by vegetation and precipitation, respectively.

3.4.3. Seasonal-scale contributions

We further analysed the seasonal-scale contribution based on the baseline simulation and the four detrended simulations. In addition to the average contribution over the Loess Plateau, we also calculated the contributions for the five subregions because of their varying climate and vegetation conditions. The absolute value of the contribution greater than 3 mm $decade^{-1}$ is generally assumed to be the significant impact. For the entire Loess Plateau, as shown in Fig. 13a, vegetation greenness significantly increases transpiration (E_t) at rates of 4–7 mm $decade^{-1}$ throughout the growing period from May to September, but it substantially reduces soil evaporation (E_s) during this period. The precipitation change promotes E_t with a peak strength of 3 mm $decade^{-1}$ in July and August, and it also intensifies E_s for the period from March to October, while the rate is not significant (<3 mm $decade^{-1}$). The radiation forcing makes a relatively minor contribution throughout the year. Therefore, the ET increase is primarily caused by precipitation in the vegetation-growing season from May to September, with a peak contribution of 6 mm $decade^{-1}$ in July.

The seasonal-scale contribution shows spatial variability in the study area. The effect of vegetation greenness is strongest in the subregions of MLP and ELP, where the LAI and FVC present larger increases than the other subregions. In the MLP, vegetation transpiration is enhanced due to greenness; particularly in July and August, the greenness-induced E_t increase is up to 14 mm $decade^{-1}$, along with an E_s decrease of approximately − 10 mm $decade^{-1}$. A similar pattern appears in the ELP, but the peak of increased E_t and decreased E_s only occur in July. The change in E_c is only driven by vegetation greenness in all five subregions, and the change in E_{sn} is not observable due to its relatively small variation.

4. Discussion

4.1. Estimation and variation of ET and its components

Partitioning ET is quite challenging partly because of limited ground-based observations, and different algorithms or products may provide different estimates, so substantial uncertainty exists and it is difficult to find “the best model” which is defined with the highest accuracy for estimating ET components. This study estimated ET and its components

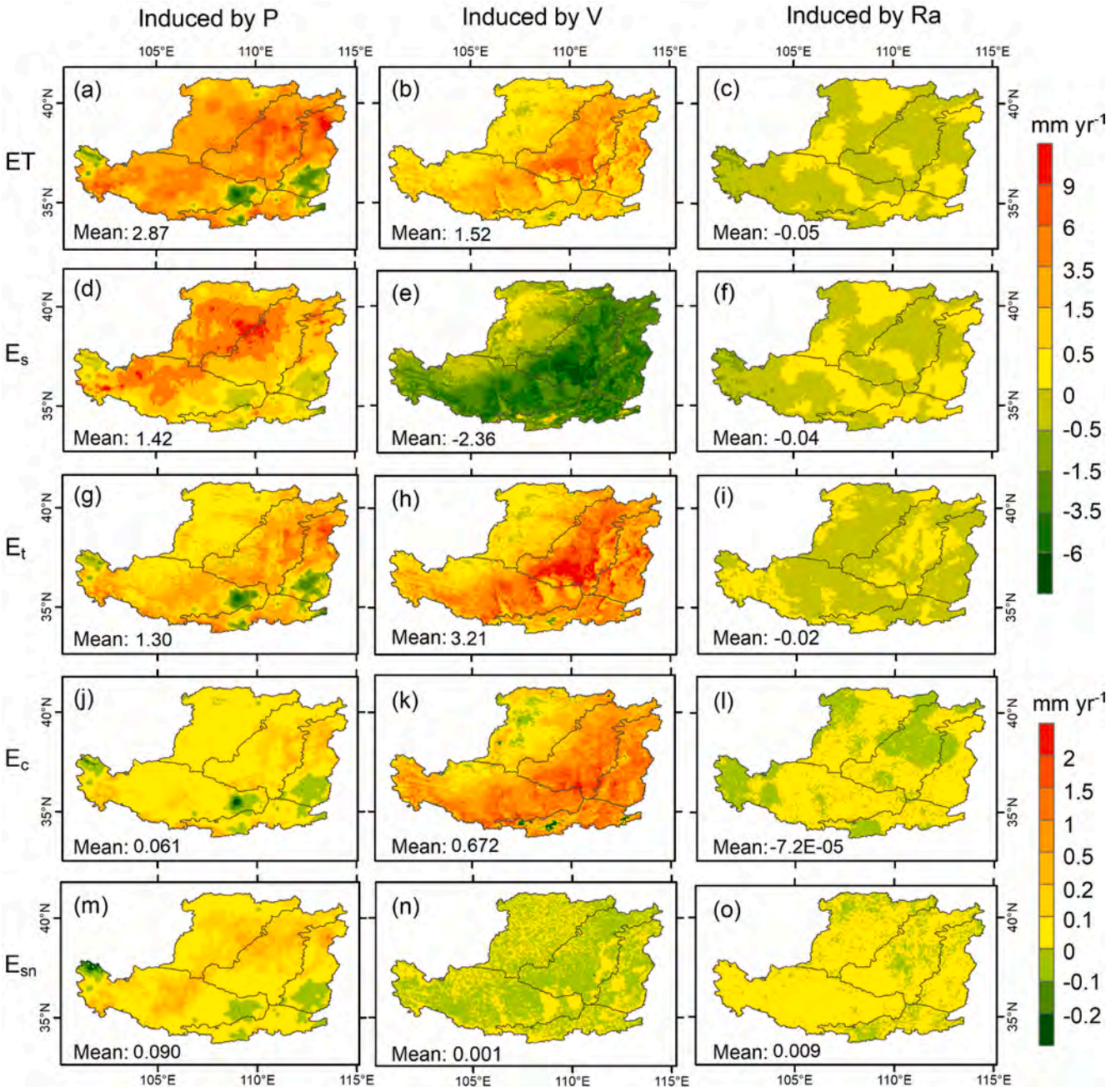

Fig. 12. Contributions of precipitation (P), vegetation (V) and radiation (Ra) to ET and the four components: (a), (b), and (c) to ET; (d), (e), and (f) to soil evaporation (E_s); (g), (h), and (i) to transpiration (E_t); (j), (k), and (l) to canopy interception loss (E_c); and (m), (n), and (o) to snow sublimation (E_{sn}). Please note that the color scale for the contributions to E_c and E_{sn} is different for the other three variables (i.e., ET, E_t, and E_s).

based on the VIC model, which is sophisticated in considering energy balance and water constraints. In the modelling, we employed remote sensing-based radiation products, including the downward shortwave and longwave radiation and land surface albedo. Moreover, the remote sensing data of LAI and FVC products were used to represent vegetation dynamics. Benefited from the integration of these remote sensing products, the hydrological modelling in this study was capable of capturing the dynamics of the four ET components along with vegetation restoration on the Loess Plateau, as evidenced by reference data of ET components from ground-based observations and remote sensing-based products.

Based on effective modelling, this study quantified the variation in ET components after ecological restoration. The results showed that ET mostly came from E_s, about 60%, roughly twice the magnitude from E_t during 2000–2018. This ratio was reasonable, as the fractional vegetation coverage was still relatively low (<20%) in the study area even after vegetation restoration programs (Fig. 11e). The largest ratio of E_s occurred in the NLP and WLP, where fractional vegetation coverage was<0.1 (Mu et al., 2021), while the highest ratio of E_t appeared in the ELP and eastern part of the MLP and WLP, where the land cover was primarily forests (Fig. 1b). A similar pattern in which E_s accounted for a larger proportion of ET than E_t was detected by Liang et al. (2020), who used a Penman-Monteith based model to simulate ET components.

This study showed that the total ET exhibited a significant upward trend, which was consistent with previous studies (Li et al., 2021b; Ning et al., 2020; Zhang et al., 2016a; Zhao et al., 2021; Zheng et al., 2019). Moreover, the vegetation-related evaporation, i.e., E_t and E_c, increased at rates of 4.76 and 0.91 mm yr^{-1}, respectively, in the study period.

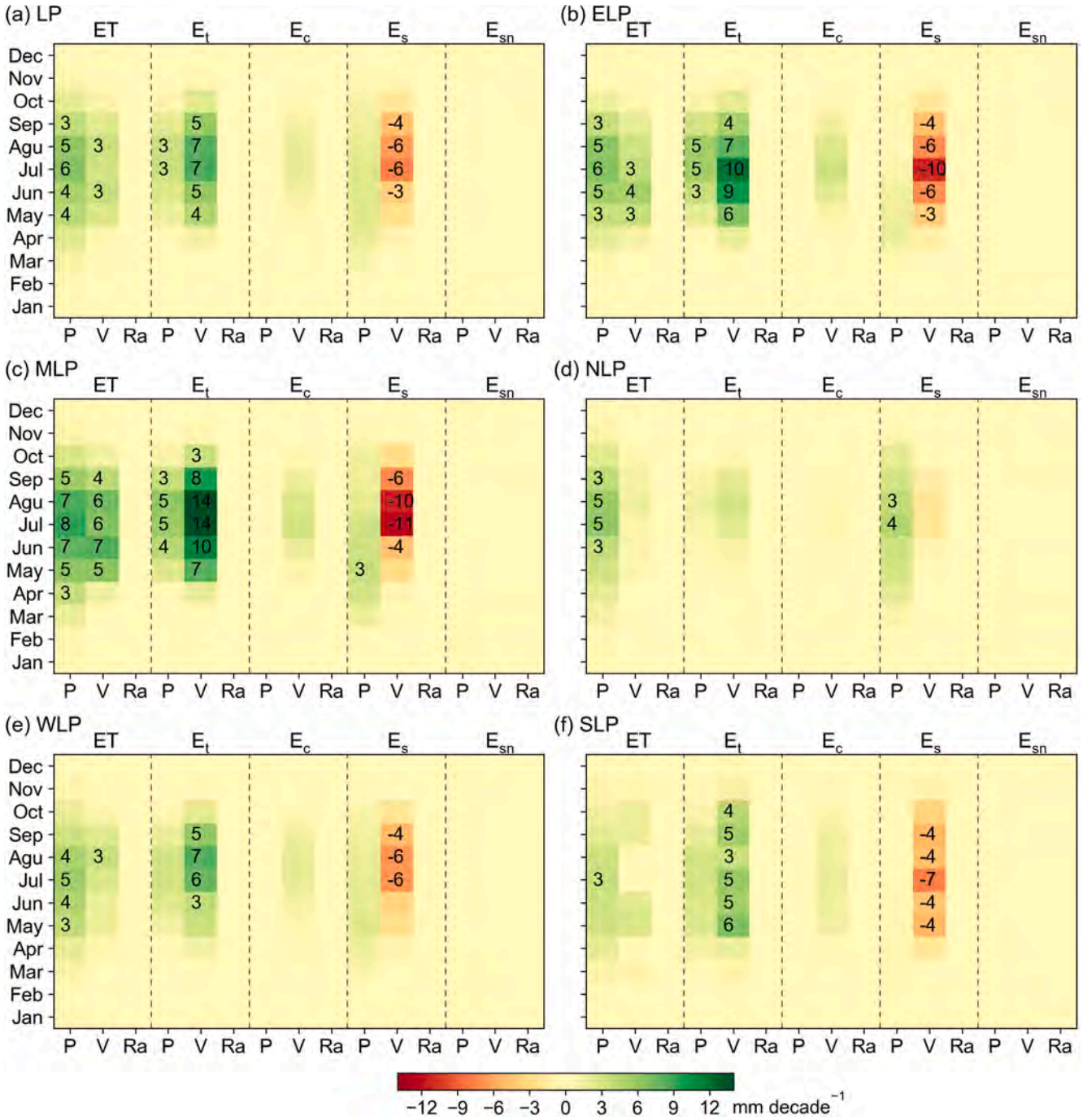

Fig. 13. Seasonal contributions of precipitation (P), vegetation (V) and radiation (Ra) to ET and its components on the Loess Plateau (LP) and the five subregions: (a) LP; (b) ELP; (c) MLP; (d) NLP; (e) WLP; and (f) SLP. Only the large numbers (absolute values greater than 3 mm decade^{-1}) are shown to denote significant contributions.

Therefore, the ratio of E_t (E_t/ET) showed a rising trend. The increasing trends of E_t and E_c were also found by Liang et al. (2020) and Shao et al. (2019). However, we found that the trend of E_s in this study also showed a slight increase of 0.09 mm yr^{-1}, which was inconsistent with the studies mentioned above. This was partly because these studies failed to consider water constraints in ET estimation, and they focused on different periods. Despite the very small increase in annual E_s during 2000–2018, the ratio of E_s (E_s/ET) showed a substantial downward trend of − 7.67% decade^{-1}.

Our study also identified the seasonal cycle of ET and its components in different stages of ecological restoration, which has usually been ignored in other studies. ET rose in all months, which perhaps affected humidity and soil moisture to some extent, and in the recent stage, E_t exceeded E_s, becoming the main component in ET from June to September due to vegetation greenness (Chen et al., 2019). E_{sn} decreased by 14% in January because of the warming climate (Sun et al., 2015).

4.2. Divergent response to vegetation greening

Previous studies have investigated the dominant factors influencing ET processes on the Loess Plateau, such as large-scale afforestation (Lv et al., 2019; Zhao et al., 2017) and precipitation (He et al., 2019; Meng et al., 2020). Given the distinct arguments and divergent response of ET

components to climatic factors and vegetation variables, our study fully explored the changes in the dominant factors of the components during 2000–2018. There is no doubt that the Loess Plateau has experienced a greening trend in recent years. Vegetation greenness enhances leaf area in regard to transpiration, but reduces the area for soil evaporation. Moreover, vegetation coverage prevents direct solar radiation forcing, thereby reducing land surface temperature. We found that vegetation greenness had a differential influence on vegetation-associated evaporation (E_t and E_c) and soil evaporation (E_s), whereas the total contribution to ET was moderate. Specifically, the vegetation greenness intensified E_t and E_c at rates of 3.21 and 0.672 mm yr^{-1}, respectively, which was mostly counteracted by the contrasting trend of E_s, approximately − 2.36 mm yr^{-1}. Moreover, it is known that precipitation variability largely influences seasonal and annual ET dynamics in water-limited areas. As a typical dryland, the Loess Plateau has increased precipitation after 2000, which has also been reported by other studies (Gao et al., 2020; Li et al., 2021a; Liu et al., 2016; Shao et al., 2019). Therefore, water availability should be the major factor driving ET changes. The results in this study confirmed that precipitation changes instead of vegetation greenness led to the increasing ET trend after ecological restoration.

We noticed the above findings are different from other studies in which land-use change was assumed to be the primary cause for the ET increase (e.g., Feng et al., 2016). The differences may stem from the study period, the method for ET calculation and the attribution analysis. First, annual precipitation has a slight increase (0.37 mm yr^{-1}) during the first decade of the revegetation, which is the period focused in precious studies, but a relatively larger increase (4.66 mm yr^{-1}) during 2000–2018. Second, Feng et al. (2016) indicated that "Annual ET estimated from the areas without revegetation does not show any significant trend". However, this is not true for the period of 2000–2018. We calculated ET for three typical land cover types, i.e., cropland, forest and grassland, based on the estimates from VIC, PML and GLEAM. We can see that ET in cropland has an obvious increase, and the change rate is larger than that in the forest (Fig. 14). So the area without land-use change (e.g. cropland) contributed substantial water consumption because the cropland area (2.016×10^5 km^2) is larger than the forest area (0.946×10^5 km^2) (Fig. 14d). Third, the methods for the ET calculation are different: our study calculated ET based on the VIC model which can consider water and energy balance; Feng et al. (2016) used satellite-derived ET which failed to consider water constraints, despite its acceptable performance. Moreover, FVC was used to drive VIC model, which is important to partition ET. The average FVC for the period was only 15%, so soil evaporation may be the primary contributor to water consumption. Our study is partly dedicated to updating findings from previous studies for the cause of the increased ET, and we argue that the effect of vegetation greening on water consumption was overestimated to a certain degree.

In addition to vegetation and precipitation, this study identified the impact of radiation forcing and provided implications for the VPD. Although downward longwave radiation has been strengthened since 1990 (Wei et al., 2021), and so did downward shortwave radiation (Yang et al., 2018), our study discovered that radiation changes had little impact on ET and its components. This has been partly demonstrated in Jiang et al. (2021) who focused on the wet season ET and indicated that ET on the Loess Plateau has intensified by approximately 5%. Moreover, we found that ET increased at a rate of 5.73 mm yr^{-1}, which was larger than the total contribution (4.34 mm yr^{-1}) from precipitation, vegetation and radiation. Therefore, we inferred that VPD might contribute to an increase in ET, while our study did not isolate the impact of VPD, which was a consequence of the air temperature and humidity, and the ET response varied due to the climate, photosynthesis strategy, and plant type (Massmann et al., 2019).

4.3. Implications and future work

The relative importance of E_t and E_s is highly dependent on vegetation coverage and water availability. However, hydrological modelling generally does not consider transient vegetation coverage information (Liu et al., 2018). Most satellite-based ET estimations lack

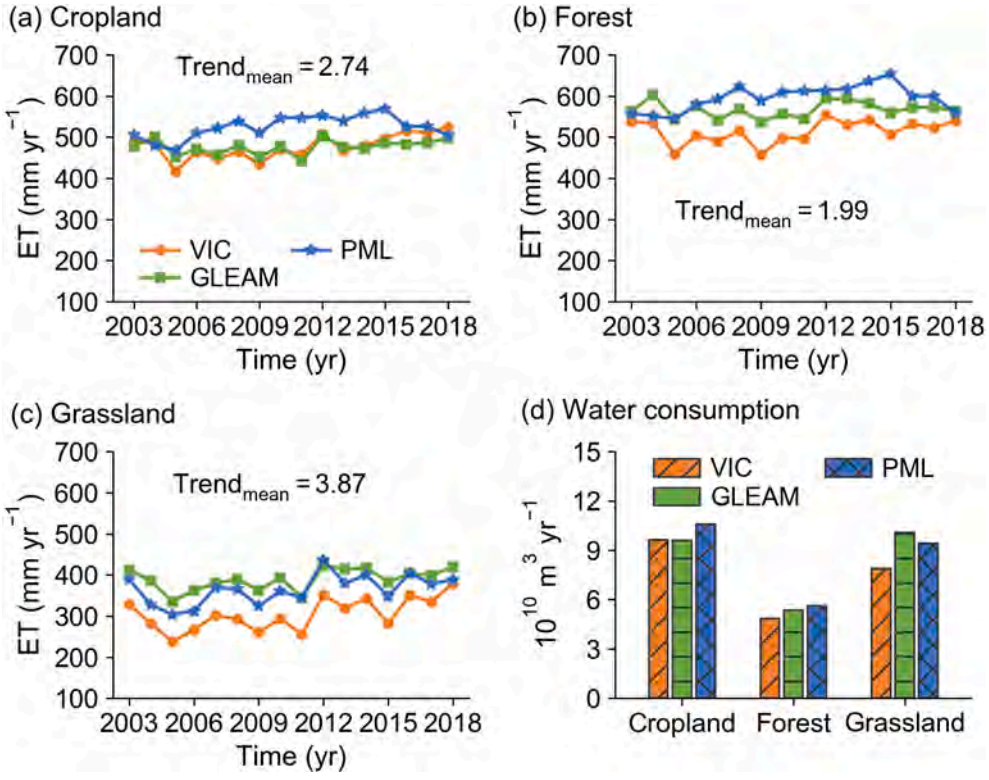

Fig. 14. Temporal changes of ET in four dominant land cover types: (a) Cropland, (b) Forest, and (c) Grassland. (d) Water consumption.

water balance constraints due to reliable soil moisture data availability (Reitz et al., 2017; Yan et al., 2012; Zhao et al., 2022). When evaluating ET in arid and semiarid regions, this study indicated that E_s rather than E_t is the primary component in ET. This relative role implies that when partitioning the ET components, it is important to consider water balance constraints and to include the dynamic fraction of vegetation coverage, and not only the LAI.

Our study has implications for evaluating water consumption in areas with vegetation greening. Many national and international ecological programs have been launched for biodiversity conservation, climate change mitigation and desertification reversion (Malagnoux et al., 2007; Strassburg et al., 2020). Revegetation is expected to increase vegetation greenness and to consequently disturb the hydrological cycle by reshaping ET processes. A few studies have concluded that afforestation or revegetation might be responsible for exacerbating water scarcity in water-limited areas worldwide (Bai et al., 2019; Deng et al., 2020; Olivera-Guerra et al., 2022; Paiva Alcoforado Rebello et al., 2020; Ukkola et al., 2016). Vegetation greenness has the potential to aggravate water shortages, with water resources reaching the limit on the Loess Plateau (Feng et al., 2016; Han et al., 2020; Li et al., 2019). However, our study demonstrates that the water consumption by vegetation greenness on the Loess Plateau may be overestimated because vegetation greenness constrained E_s along with the increased E_t. In this arid and semiarid region, E_s is still the primary component of water consumption. The increased ET is primarily caused by water availability, i.e., increasing precipitation. Please note that the findings from this study do not contradict that vegetation greenness is partly responsible for the increased ET. Vegetation greenness promotes more transpiration than water availability does. Moreover, transpiration on the Loess Plateau is becoming a primary component approximately equal to or larger than soil evaporation. We argue that there is a caveat for evaluating the hydrological effect of vegetation greenness. Particularly, it is important to avoid the overestimation by considering the counterbalance between vegetation transpiration and soil evaporation.

There are future works needed to address the hydrological effect of vegetation greenness. This study provided an example of water consumption in a typical dryland. ET consumption highly depends on the magnitude of greening, climate conditions, and radiation forcing. Therefore, it would be a good attempt to characterize the hydrological effect in different regions or at the global scale with varying greenness. Moreover, the climate system and vegetation have strong interactions (Zeng and Neelin, 2000); for example, drought had a lagged effect on vegetation growth (Wu et al., 2020). Neglecting this interaction would cause uncertainties. In addition, vegetation greenness generates more litter coverage, which plays an important role in the hydrological cycle. The litter layer can affect root water uptake, soil moisture evaporation and drainage to mineral soils (Du et al., 2019). In hydrological modelling, it would be important to consider the hydrological effect of litter coverage to achieve a holistic evaluation of vegetation greenness.

5. Conclusions

In this study, we examined ET components in response to vegetation greening in a typical dryland, i.e., the Loess Plateau in China. The four ET components (E_t, E_c, E_s, and E_{sn}) were successfully estimated based on sophisticated land surface hydrological modelling, i.e., VIC model, which was featured by consideration of water and energy balance with transient vegetation structure and coverage constraints. Contrasting to conventional hydrological modelling, newly released long-term satellite products (e.g., FVC, LAI and radiation parameters) were integrated into this model to estimate ET components. The modelling achieved reliable estimation of the ET components as evaluated using ground-based observations and remote sensing-based data. Based on hydrological modelling, this study achieved a few interesting conclusions:

(1) Soil evaporation (E_s) accounted for approximately 60% of ET, which was much larger than the vegetation transpiration (E_t) during the vegetation greening period of 2000–2018. So the water consumption on the Loess Plateau was primarily from E_s rather than E_t.
(2) Despite a slight increase in E_s, its ratio of E_s/ET decreased at a rate of $-$ 7.67% decade^{-1}, along with a similar level of increase in E_t. Therefore, E_t overtook E_s, becoming the main component of ET currently in the warm season from June to September.
(3) Vegetation greenness substantially caused E_s to decline at a rate of $-$ 2.36 mm yr^{-1}, implying that vegetation greening constrained E_s because vegetation coverage decreased the bare soil area and reduced land surface temperature. In contrast, the increased precipitation over the Loess Plateau provided more water availability, thereby promoting all the four ET components, so it was the primary factor to promote water consumption.
(4) In the vegetation-growing season and in the concentration areas of ecological restoration, water availability was still the major contributor to intensify the total ET because of the counterbalance between E_t and E_s.

The above findings imply that the role of vegetation greenness on water consumption may be overestimated for the Loess Plateau. This does not necessarily mean that vegetation greenness is not responsible for water consumption. Global vegetation greenness will induce ET consumption with spatial–temporal variability. It would be important to revisit the effect of vegetation greenness on water consumption by considering the constraints of vegetation greenness on soil evaporation. Moreover, the water balance and the vegetation coverage magnitude should be included in ET estimation.

Declaration of Competing Interest

The authors declare that they have no known competing financial interests or personal relationships that could have appeared to influence the work reported in this paper.

Data availability

Data will be made available on request.

Acknowledgements

This study was supported by a grant from the National Natural Science Foundation of China (No. 41971030). The authors thank Prof. Chiyuan Miao for providing a few stations of water discharge data to evaluate the VIC model.

References

Adler, R.F., Gu, G., Sapiano, M., Wang, J.-J., Huffman, G.J., 2017. Global precipitation: means, variations and trends during the satellite Era (1979–2014). Surv. Geophys. 38 (4), 679–699. https://doi.org/10.1007/s10712-017-9416-4.

Althoff, D., Rodrigues, L.N., 2021. Goodness-of-fit criteria for hydrological models: Model calibration and performance assessment. J. Hydrol. 600, 126674 https://doi.org/10.1016/j.jhydrol.2021.126674.

Bai, M., Mo, X.G., Liu, S.X., Hu, S., 2019. Contributions of climate change and vegetation greening to evapotranspiration trend in a typical hilly-gully basin on the Loess Plateau. China. Sci. Total Environ. 657, 325–339. https://doi.org/10.1016/j.scitotenv.2018.11.360.

Bryan, B.A., et al., 2018. China's response to a national land-system sustainability emergency. Nature 559 (7713), 193–204. https://doi.org/10.1038/s41586-018-0280-2.

Chen, C., et al., 2019. China and India lead in greening of the world through land-use management. Nat. Sustainability 2 (2), 122–129. https://doi.org/10.1038/s41893-019-0220-7.

Chen, X., Mo, X., Hu, S., Liu, S., 2017. Contributions of climate change and human activities to ET and GPP trends over North China Plain from 2000 to 2014. J. Geog. Sci. 27 (6), 661–680. https://doi.org/10.1007/s11442-017-1399-z.

Deng, Y., et al., 2020. Vegetation greening intensified soil drying in some semi-arid and arid areas of the world. Agric. For. Meteorol. 292–293, 108103 https://doi.org/10.1016/j.agrformet.2020.108103.
Du, J., et al., 2019. Effects of rainfall intensity and slope on interception and precipitation partitioning by forest litter layer. CATENA 172, 711–718. https://doi.org/10.1016/j.catena.2018.09.036.
Duveiller, G., Hooker, J., Cescatti, A., 2018. The mark of vegetation change on Earth's surface energy balance. Nat. Commun. 9 (1), 679. https://doi.org/10.1038/s41467-017-02810-8.
Fan, X., et al., 2015. Land use/land cover changes and regional climate over the Loess Plateau during 2001–2009. Part I: observational evidence. Clim. Change 129 (3), 427–440. https://doi.org/10.1007/s10584-014-1069-4.
Feng, X.M., et al., 2012. Regional effects of vegetation restoration on water yield across the Loess Plateau. China. Hydrol. Earth Syst. Sci. 16 (8), 2617–2628. https://doi.org/10.5194/hess-16-2617-2012.
Feng, X.M., et al., 2016. Revegetation in China's Loess Plateau is approaching sustainable water resource limits. Nat. Clim. Change 6 (11), 1019-+. https://doi.org/10.1038/nclimate3092.
Fisher, J.B., Tu, K.P., Baldocchi, D.D., 2008. Global estimates of the land–atmosphere water flux based on monthly AVHRR and ISLSCP-II data, validated at 16 FLUXNET sites. Remote Sens. Environ. 112 (3), 901–919. https://doi.org/10.1016/j.rse.2007.06.025.
Gao, X., et al., 2017. Actual ET modelling based on the Budyko framework and the sustainability of vegetation water use in the loess plateau. Sci. Total Environ. 579, 1550–1559. https://doi.org/10.1016/j.scitotenv.2016.11.163.
Gao, X.R., et al., 2020. The spatial and temporal evolution of the actual evapotranspiration based on the remote sensing method in the Loess Plateau. Sci. Total Environ. 708 https://doi.org/10.1016/j.scitotenv.2019.135111.
Gu, G., 2016. Long-term changes/trends in surface temperature and precipitation during the satellite era (1979–2012). Clim. Dyn. 46, 1091–1105. https://doi.org/10.1007/s00382-015-2634-x.
Gupta, H.V., Kling, H., Yilmaz, K.K., Martinez, G.F., 2009. Decomposition of the mean squared error and NSE performance criteria: Implications for improving hydrological modelling. J. Hydrol. 377 (1), 80–91. https://doi.org/10.1016/j.jhydrol.2009.08.003.
Haddeland, I., Lettenmaier, D.P., Skaugen, T., 2006. Effects of irrigation on the water and energy balances of the Colorado and Mekong river basins. J. Hydrol. 324 (1), 210–223. https://doi.org/10.1016/j.jhydrol.2005.09.028.
Han, Z., et al., 2020. Effects of vegetation restoration on groundwater drought in the Loess Plateau. China. J. Hydrol. 591, 125566 https://doi.org/10.1016/j.jhydrol.2020.125566.
He, G., et al., 2019. Attribution analysis based on Budyko hypothesis for land evapotranspiration change in the Loess Plateau, China. J. Arid Land 11 (6), 939–953. https://doi.org/10.1007/s40333-019-0107-5.
He, J., et al., 2020. The first high-resolution meteorological forcing dataset for land process studies over China. Sci. Data 7 (1), 25. https://doi.org/10.1038/s41597-020-0369-y.
He, B., Chen, A.F., Wang, H.L., Wang, Q.F., 2015. Dynamic response of satellite-derived vegetation growth to climate change in the three north shelter forest region in China. Remote Sens. 7 (8), 9998–10016. https://doi.org/10.3390/rs70809998.
Hu, Z., et al., 2008. Effects of vegetation control on ecosystem water use efficiency within and among four grassland ecosystems in China. Global Change Biol. 14 (7), 1609–1619. https://doi.org/10.1111/j.1365-2486.2008.01582.x.
Jia, K., et al., 2015. Global land surface fractional vegetation cover estimation using general regression neural networks from MODIS surface reflectance. IEEE Trans. Geosci. Remote Sens. 53 (9), 4787–4796. https://doi.org/10.1109/tgrs.2015.2409563.
Jia, X.X., Shao, M.A., Zhu, Y.J., Luo, Y., 2017. Soil moisture decline due to afforestation across the Loess Plateau. China. J. Hydrol. 546, 113–122. https://doi.org/10.1016/j.jhydrol.2017.01.011.
Jiang, F., et al., 2021. Loess Plateau evapotranspiration intensified by land surface radiative forcing associated with ecological restoration. Agric. For. Meteorol. 311, 108669 https://doi.org/10.1016/j.agrformet.2021.108669.
Jiao, L., et al., 2018. Evapotranspiration partitioning and its implications for plant water use strategy: Evidence from a black locust plantation in the semi-arid Loess Plateau. China. For. Ecol. Manage. 424, 428–438. https://doi.org/10.1016/j.foreco.2018.05.011.
Jiao, L., Lu, N., Sun, G., Ward, E.J., Fu, B., 2016. Biophysical controls on canopy transpiration in a black locust (Robinia pseudoacacia) plantation on the semi-arid Loess Plateau. China. Ecohydrol. 9 (6), 1068–1081. https://doi.org/10.1002/eco.1711.
Jung, M., et al., 2010. Recent decline in the global land evapotranspiration trend due to limited moisture supply. Nature 467 (7318), 951–954. https://doi.org/10.1038/nature09396.
Law, B.E., et al., 2002. Environmental controls over carbon dioxide and water vapor exchange of terrestrial vegetation. Agric. For. Meteorol. 113 (1), 97–120. https://doi.org/10.1016/S0168-1923(02)00104-1.
Lawrence, D.M., Thornton, P.E., Oleson, K.W., Bonan, G.B., 2007. The partitioning of evapotranspiration into transpiration, soil evaporation, and canopy evaporation in a GCM: impacts on land-atmosphere interaction. J. Hydrometeorol. 8 (4), 862–880. https://doi.org/10.1175/JHM596.1.
Li, T., et al., 2021b. An improved complementary relationship for estimating evapotranspiration attributed to climate change and revegetation in the Loess Plateau. China. J. Hydrol. 592, 125516 https://doi.org/10.1016/j.jhydrol.2020.125516.
Li, Y., Mao, D., Feng, A., Schillerberg, T., 2019. Will Human-Induced Vegetation Regreening Continually Decrease Runoff in the Loess Plateau of China? Forests 10 (10). https://doi.org/10.3390/f10100906.
Li, B., Yang, Y., Li, Z., 2021a. Combined effects of multiple factors on spatiotemporally varied soil moisture in China's Loess Plateau. Agric. Water Manage. 258, 107180 https://doi.org/10.1016/j.agwat.2021.107180.
Liang, S., et al., 2013. A long-term Global LAnd Surface Satellite (GLASS) data-set for environmental studies. Int. J. Digital Earth 6 (sup1), 5–33. https://doi.org/10.1080/17538947.2013.805262.
Liang, S., et al., 2021. The Global Land Surface Satellite (GLASS) Product Suite. Bull. Am. Meteorol. Soc. 102 (2), E323–E337. https://doi.org/10.1175/BAMS-D-18-0341.1.
Liang, W., et al., 2020. Rapid urbanization and agricultural intensification increase regional evaporative water consumption of the Loess Plateau. e2020JD033380 J. Geophys. Res.: Atmos. 125 (23). https://doi.org/10.1029/2020JD033380.
Liang, X., Lettenmaier, D.P., Wood, E.F., Burges, S.J., 1994. A simple hydrologically based model of land surface water and energy fluxes for general circulation models. J. Geophys. Res.: Atmos. 99 (D7), 14415–14428. https://doi.org/10.1029/94jd00483.
Liang, X., Wood, E.F., Lettenmaier, D.P., 1996. Surface soil moisture parameterization of the VIC-2L model: Evaluation and modification. Global Planet. Change 13 (1), 195–206. https://doi.org/10.1016/0921-8181(95)00046-1.
Liu, J.L., 2008. A study on the Hillslope ecohydrological processes and vegetation carrying capacity in the small catchment of Diediegou, Liupanshan Mountain. Chin. Acad. Forest.
Liu, J.Y., et al., 2010. Spatial patterns and driving forces of land use change in China during the early 21st century. J. Geog. Sci. 20 (4), 483–494. https://doi.org/10.1007/s11442-010-0483-4.
Liu, Q., et al., 2013. Preliminary evaluation of the long-term GLASS albedo product. Int. J. Digital Earth 6 (sup1), 69–95. https://doi.org/10.1080/17538947.2013.804601.
Liu, Y., et al., 2016. Recent trends in vegetation greenness in China significantly altered annual evapotranspiration and water yield. Environ. Res. Lett. 11 (9), 094010 https://doi.org/10.1088/1748-9326/11/9/094010.
Liu, M., Adam, J.C., Richey, A.S., Zhu, Z., Myneni, R.B., 2018. Factors controlling changes in evapotranspiration, runoff, and soil moisture over the conterminous U.S.: Accounting for vegetation dynamics. J. Hydrol. 565, 123–137. https://doi.org/10.1016/j.jhydrol.2018.07.068.
Liu, Z., Wang, J., Wang, X., Wang, Y., 2020. Understanding the impacts of 'Grain for Green' land management practice on land greening dynamics over the Loess Plateau of China. Land Use Policy 99, 105084. https://doi.org/10.1016/j.landusepol.2020.105084.
Lv, X., Zuo, Z., Sun, J., Ni, Y., Wang, Z., 2019. Climatic and human-related indicators and their implications for evapotranspiration management in a watershed of Loess Plateau. China. Ecol. Indic. 101, 143–149. https://doi.org/10.1016/j.ecolind.2019.01.019.
Ma, H., Liang, S., 2022. Development of the GLASS 250-m leaf area index product (version 6) from MODIS data using the bidirectional LSTM deep learning model. Remote Sens. Environ. 273, 112985 https://doi.org/10.1016/j.rse.2022.112985.
Ma, W., Wei, Z., Wang, P., Asanuma, J., 2020. Transpiration and evaporation of grassland using land surface modelling. Hydrol. Processes 34 (17), 3656–3668. https://doi.org/10.1002/hyp.13792.
Malagnoux, M., Sene, E.H., Atzmon, N., 2007. Forests, trees and water in arid lands: a delicate balance. Unasylva 58.
Mao, J., et al., 2015. Disentangling climatic and anthropogenic controls on global terrestrial evapotranspiration trends. Environ. Res. Lett. 10 (9), 094008 https://doi.org/10.1088/1748-9326/10/9/094008.
Martens, B., et al., 2017. GLEAM v3: satellite-based land evaporation and root-zone soil moisture. Geosci. Model Dev. 10 (5), 1903–1925. https://doi.org/10.5194/gmd-10-1903-2017.
Massmann, A., Gentine, P., Lin, C., 2019. When does vapor pressure deficit drive or reduce evapotranspiration? J. Adv. Model. Earth Syst. 11 (10), 3305–3320. https://doi.org/10.1029/2019MS001790.
Meng, S., Xie, X., Zhu, B., Wang, Y., 2020. The relative contribution of vegetation greening to the hydrological cycle in the Three-North region of China: A modelling analysis. J. Hydrol. 591, 125689 https://doi.org/10.1016/j.jhydrol.2020.125689.
Miralles, D.G., et al., 2011. Global land-surface evaporation estimated from satellite-based observations. Hydrol. Earth Syst. Sci. 15 (2), 453–469. https://doi.org/10.5194/hess-15-453-2011.
Monteith, J.L., 1965. Evaporation and environment. Symp. Soc. Experiment. Biol. 19, 205–234.
Mu, B.H., et al., 2021. Vegetation cover change and its attribution in China from 2001 to 2018. Remote Sens. 13 (3), 17. https://doi.org/10.3390/rs13030496.
Nijssen, B., Schnur, R., Lettenmaier, D.P., 2001. Global retrospective estimation of soil moisture using the variable infiltration capacity land surface model, 1980–93. J. Clim. 14 (8), 1790–1808. https://doi.org/10.1175/1520-0442(2001)014<1790:GREOSM>2.0.CO;2.
Ning, T., Liu, W., Li, Z., Feng, Q., 2020. Modelling and attributing evapotranspiration changes on China's Loess Plateau with Budyko framework considering vegetation dynamics and climate seasonality. Stochastic Environ. Res. Risk Assess. 34 (8), 1217–1230. https://doi.org/10.1007/s00477-020-01813-0.
Oki, T., Kanae, S., 2006. Global hydrological cycles and world water resources. Science 313 (5790), 1068–1072. https://doi.org/10.1126/science.1128845.
Olivera-Guerra, L., et al., 2022. Water dynamics over a Western Patagonian watershed: Land surface changes and human factors. Sci. Total Environ. 804, 150221 https://doi.org/10.1016/j.scitotenv.2021.150221.

Painter, T.H., et al., 2010. Response of Colorado River runoff to dust radiative forcing in snow. Proc. Natl. Acad. Sci. U.S.A. 107 (40), 17125. https://doi.org/10.1073/pnas.0913139107.
Pan, S., et al., 2015. Responses of global terrestrial evapotranspiration to climate change and increasing atmospheric CO2 in the 21st century. Earth's Future 3 (1), 15–35. https://doi.org/10.1002/2014EF000263.
Peng, S.Z., Gang, C.C., Cao, Y., Chen, Y.M., 2018. Assessment of climate change trends over the Loess Plateau in China from 1901 to 2100. Int. J. Climatol. 38 (5), 2250–2264. https://doi.org/10.1002/joc.5331.
Penman, H.L., Keen, B.A., 1948. Natural evaporation from open water, bare soil and grass. Proc. R. Soc. London, Ser. A 193 (1032), 120–145. https://doi.org/10.1098/rspa.1948.0037.
Piao, S., et al., 2020. Characteristics, drivers and feedbacks of global greening. Nat. Rev. Earth Environ. 1 (1), 14–27. https://doi.org/10.1038/s43017-019-0001-x.
Qiu, L., Wu, Y., Shi, Z., Chen, Y., Zhao, F., 2021. Quantifying the responses of evapotranspiration and its components to vegetation restoration and climate change on the Loess Plateau of China. Remote Sens. 13 (12) https://doi.org/10.3390/rs13122358.
Paiva Alcoforado Rebello, V., Getirana, A., Rotunno Filho, O.C., Lakshmi, V., 2020. Spatiotemporal vegetation response to extreme droughts in eastern Brazil. Remote Sens. Appl.: Soc. Environ. 18, 100294 https://doi.org/10.1016/j.rsase.2020.100294.
Reitz, M., Senay, G.B., Sanford, W.E., 2017. Combining remote sensing and water-balance evapotranspiration estimates for the conterminous United States. Remote Sens. 9 (12) https://doi.org/10.3390/rs9121181.
Schlesinger, W.H., Jasechko, S., 2014. Transpiration in the global water cycle. Agric. For. Meteorol. 189–190, 115–117. https://doi.org/10.1016/j.agrformet.2014.01.011.
Shao, R., et al., 2019. Estimating the increase in regional evaporative water consumption as a result of vegetation restoration over the Loess Plateau. China. J. Geophys. Res.: Atmos. 124 (22), 11783–11802. https://doi.org/10.1029/2019JD031295.
Shi, X., Mao, J., Thornton, P.E., Huang, M., 2013. Spatiotemporal patterns of evapotranspiration in response to multiple environmental factors simulated by the Community Land Model. Environ. Res. Lett. 8 (2), 024012 https://doi.org/10.1088/1748-9326/8/2/024012.
Shuttleworth, W., 1993. Evaporation. In: Maidment, D.R. (Ed.), Handbook of Hydrology. McGraw-Hill New York.
Strassburg, B.B.N., et al., 2020. Global priority areas for ecosystem restoration. Nature 586 (7831), 724–729. https://doi.org/10.1038/s41586-020-2784-9.
Sun, Q., Miao, C., Duan, Q., Wang, Y., 2015. Temperature and precipitation changes over the Loess Plateau between 1961 and 2011, based on high-density gauge observations. Global Planet. Change 132, 1–10. https://doi.org/10.1016/j.gloplacha.2015.05.011.
Tian, J.H., 2005. Studies on Water Consumption Characteristics of Main Tree Species Of Soil And Water Conservation Forest In Semi-Arid Region On the Loess Plateau. Beijing Forestry University.
Ukkola, A.M., Keenan, T.F., Kelley, D.I., Prentice, I.C., 2016. Vegetation plays an important role in mediating future water resources. Environ. Res. Lett. 11 (9), 094022 https://doi.org/10.1088/1748-9326/11/9/094022.
Wang, K., Liang, S., 2009. Global atmospheric downward longwave radiation over land surface under all-sky conditions from 1973 to 2008. J. Geophys. Res.: Atmos. 114 (D19) https://doi.org/10.1029/2009JD011800.
Wang, X., Zhang, B., Xu, X., Tian, J., He, C., 2020. Regional water-energy cycle response to land use/cover change in the agro-pastoral ecotone. Northwest China. J. Hydrol. 580, 124246 https://doi.org/10.1016/j.jhydrol.2019.124246.
Wei, Y., et al., 2021. Trends and Variability of Atmospheric Downward Longwave Radiation Over China From 1958 to 2015. Earth Space Sci. 8 (2) https://doi.org/10.1029/2020EA001370 e2020EA001370.
Wilcox, B., Breshears, D., Seyfried, M., 2003. Rangelands, Water Balance on. Encyclopedia of Water Science.
Wild, M., 2016. Decadal changes in radiative fluxes at land and ocean surfaces and their relevance for global warming. WIREs Clim. Change 7 (1), 91–107. https://doi.org/10.1002/wcc.372.
Wu, D.D., Xie, X.H., Tong, J.X., Meng, S.S., Wang, Y.B., 2020. Sensitivity of Vegetation Growth to Precipitation in a Typical Afforestation Area in the Loess Plateau: Plant-Water Coupled Modelling. Ecol. Modell. 430, 14. https://doi.org/10.1016/j.ecolmodel.2020.109128.
Xiao, Z.Q., et al., 2014. Use of general regression neural networks for generating the GLASS leaf area index product from time-series MODIS surface reflectance. IEEE Trans. Geosci. Remote Sens. 52 (1), 209–223. https://doi.org/10.1109/tgrs.2013.2237780.
Xie, X., et al., 2015. Detection and attribution of changes in hydrological cycle over the Three-North region of China: Climate change versus afforestation effect. Agric. For. Meteorol. 203, 74–87. https://doi.org/10.1016/j.agrformet.2015.01.003.
Xie, S., Mo, X., Hu, S., Liu, S., 2020. Contributions of climate change, elevated atmospheric CO2 and human activities to ET and GPP trends in the Three-North Region of China. Agric. For. Meteorol. 295, 108183 https://doi.org/10.1016/j.agrformet.2020.108183.
Yan, H., et al., 2012. Global estimation of evapotranspiration using a leaf area index-based surface energy and water balance model. Remote Sens. Environ. 124, 581–595. https://doi.org/10.1016/j.rse.2012.06.004.
Yang, K., He, J., Tang, W., Qin, J., Cheng, C.C.K., 2010. On downward shortwave and longwave radiations over high altitude regions: Observation and modeling in the Tibetan Plateau. Agric. For. Meteorol. 150 (1), 38–46. https://doi.org/10.1016/j.agrformet.2009.08.004.
Yang, S., Wang, X.L., Wild, M., 2018. Homogenization and Trend Analysis of the 1958–2016 In Situ Surface Solar Radiation Records in China. J. Clim. 31 (11), 4529–4541. https://doi.org/10.1175/JCLI-D-17-0891.1.
Yang, Y., Wang, B., Wang, G., Li, Z., 2019. Ecological regionalization and overview of the Loess Plateau. Acta Ecol. Sin. 39 (20), 7389–7397.
Yao, Y., et al., 2019. Extended dependence of the hydrological regime on the land cover change in the three-north region of China: An evaluation under future climate conditions. Remote Sens. 11 (1) https://doi.org/10.3390/rs11010081.
Zeng, Z., et al., 2016. Responses of land evapotranspiration to Earth's greening in CMIP5 Earth System Models. Environ. Res. Lett. 11 (10), 104006 https://doi.org/10.1088/1748-9326/11/10/104006.
Zeng, N., Neelin, J.D., 2000. The role of vegetation-climate interaction and interannual variability in shaping the African Savanna. J. Clim. 13 (15), 2665–2670. https://doi.org/10.1175/1520-0442(2000)013<2665:TROVCI>2.0.CO;2.
Zeng, Z., Peng, L., Piao, S., 2018. Response of terrestrial evapotranspiration to Earth's greening. Curr. Opin. Environ. Sustain. 33, 9–25. https://doi.org/10.1016/j.cosust.2018.03.001.
Zhang, K., et al., 2015b. Vegetation greening and climate change promote multidecadal rises of global land evapotranspiration. Sci. Rep. 5 (1), 15956. https://doi.org/10.1038/srep15956.
Zhang, Y., et al., 2016b. Multi-decadal trends in global terrestrial evapotranspiration and its components. Sci. Rep. 6 (1), 19124. https://doi.org/10.1038/srep19124.
Zhang, Q., et al., 2018. Sap flow of black locust in response to short-term drought in southern Loess Plateau of China. Sci. Rep. 8 (1), 6222. https://doi.org/10.1038/s41598-018-24669-5.
Zhang, Y., et al., 2019b. Coupled estimation of 500 m and 8-day resolution global evapotranspiration and gross primary production in 2002–2017. Remote Sens. Environ. 222, 165–182. https://doi.org/10.1016/j.rse.2018.12.031.
Zhang, J.-G., Guan, J.-H., Shi, W.-Y., Yamanaka, N., Du, S., 2015a. Interannual variation in stand transpiration estimated by sap flow measurement in a semi-arid black locust plantation, Loess Plateau, China. Ecohydrology 8 (1), 137–147. https://doi.org/10.1002/eco.1495.
Zhang, X., Liang, S., Zhou, G., Wu, H., Zhao, X., 2014. Generating Global Lasnd Surface Satellite incident shortwave radiation and photosynthetically active radiation products from multiple satellite data. Remote Sens. Environ. 152, 318–332. https://doi.org/10.1016/j.rse.2014.07.003.
Zhang, T., Peng, J., Liang, W., Yang, Y., Liu, Y., 2016a. Spatial–temporal patterns of water use efficiency and climate controls in China's Loess Plateau during 2000–2010. Sci. Total Environ. 565, 105–122. https://doi.org/10.1016/j.scitotenv.2016.04.126.
Zhang, K., Xie, X., Zhu, B., Meng, S., Yao, Y., 2019a. Unexpected groundwater recovery with decreasing agricultural irrigation in the Yellow River Basin. Agric. Water Manage. 213, 858–867. https://doi.org/10.1016/j.agwat.2018.12.009.
Zhao, A., et al., 2017. Spatiotemporal variation of vegetation coverage before and after implementation of Grain for Green Program in Loess Plateau, China. Ecol. Eng. 104, 13–22. https://doi.org/10.1016/j.ecoleng.2017.03.013.
Zhao, F., et al., 2022. The role of climate change and vegetation greening on evapotranspiration variation in the Yellow River Basin, China. Agric. For. Meteorol. 316, 108842 https://doi.org/10.1016/j.agrformet.2022.108842.
Zhao, A., Yu, Q., Wang, D., Zhang, A., 2021. Spatiotemporal dynamics of ecosystem water use efficiency over the Chinese Loess Plateau base on long-time satellite data. Environ. Sci. Pollut. Res. https://doi.org/10.1007/s11356-021-15801-6.
Zheng, H., Lin, H., Zhu, X., 2019. Spatiotemporal patterns of terrestrial evapotranspiration in response to climate and vegetation coverage changes across the Chinese Loess Plateau. Water 11 (8). https://doi.org/10.3390/w11081625.
Zhu, B., et al., 2021. Extensive evaluation of a continental-scale high-resolution hydrological model using remote sensing and ground-based observations. Remote Sens. 13 (7) https://doi.org/10.3390/rs13071247.